ELSEVIER

Journal of Structural Geology 30 (2008) 159–176

JOURNAL OF STRUCTURAL GEOLOGY

www.elsevier.com/locate/jsg

Anatomy of a transitional brittle–ductile shear zone developed in a low-T meta-andesite tuff: A microstructural, petrological and geochronological case study from the Bükk Mts. (NE Hungary)

Balázs Koroknai [a,*], Péter Árkai [b], Péter Horváth [b], Kadosa Balogh [c]

[a] *Geological Institute of Hungary, Stefánia u. 14, H-1143 Budapest, Hungary*
[b] *Institute for Geochemical Research, Hungarian Academy of Sciences, Budaörsi út 45, H-1112 Budapest, Hungary*
[c] *Institute of Nuclear Research, Hungarian Academy of Sciences, Bem tér 18/c, H-4026 Debrecen, Hungary*

Received 10 July 2007; received in revised form 18 October 2007; accepted 22 October 2007
Available online 17 November 2007

Abstract

Microstructures of the low-T metavolcanites deriving from the transitional brittle–ductile Lillafüred Shear Zone (LSZ, Eastern Bükk Mts., NE Hungary) reveal that the prominent mylonitic rock-structure observed at hand-specimen scale was predominantly achieved at the grain scale by (1) intense microfracturing of rigid minerals (feldspar, opaque phases), and (2) intergranular sliding associated with solution mass transfer within the prevailing, fine-grained, phyllosilicate-rich matrix. Fluid migration during shearing—indicated by widespread growth of syntectonic, secondary calcite and pervasive retrograde alteration of feldspar into ''weak'', fine-grained mica aggregates—led to substantial weakening and localization of deformation into narrow zones. This is accompanied microstructurally by an evolution from a cataclasis-dominated regime towards a more ductile, mylonitic deformation. Various metamorphic petrological and geochronological parameters (illite Kübler index, chlorite ''crystallinity'' indices, crystallite thickness, mean lattice strain, chlorite-Al^{IV} thermometry, K-Ar ages on <2 μm white K-mica) indicate uniformly peak metamorphic conditions around the boundary of the anchi/epizone (300–350 °C) and subsequent cooling about 76 Ma both in the heavily sheared rocks of the LSZ and the enclosing, weakly deformed rock mass. These relationships suggest that the LSZ represents a late-stage, relatively ''cold'' ($\leq$250–270 °C), fluid-assisted, dextral strike-slip zone formed after 76 Ma on the retrograde path of the Eoalpine tectonometamorphic cycle.

Keywords: Brittle–ductile; Low-T shear zone; Illite Kübler index; Chlorite ''crystallinity''; K-Ar Geochronology; Bükk Mts.

1. Introduction

Primarily cohesive fault rocks formed in crustal shear zones, disregarding pseudotachylites, are broadly divided into two major categories (see e.g. Sibson, 1977; White et al., 1980; Wise et al., 1984; Schmid and Handy, 1991; and references therein): ''classical'' cataclasites with a general random, unfoliated fabric formed basically by brittle (frictional) processes prevail in upper crustal shear zones (<8–10 km), whereas typical mylonites with prominent foliation and associated stretching lineation occur at mid- to lower crustal levels, where thermally activated viscous deformation mechanisms (e.g. crystal plasticity, diffusional creep) predominate in the rock matrix. However, a wide transitional range exists between these two ''end-members'', where both frictional and viscous deformation mechanisms may operate simultaneously. Foliated fault rocks deriving from this transitional range characterized by (very) low-T metamorphic conditions may be also of cataclastic origin (e.g. Chester et al., 1985; Lin, 1997, 1999). Nevertheless, interpretation of such tectonites needs special care, as the common (ultra)fine grain-size of the rock matrix—composed of mainly phyllosilicates in many cases—largely handicaps the identification of active grain-scale deformation mechanisms. Optical

* Corresponding author. Tel./fax: +36 1 251 7678.
E-mail addresses: koroknai@mafi.hu (B. Koroknai), arkai@geochem.hu (P. Árkai), phorvath@geochem.hu (P. Horváth), balogh@atomki.hu (K. Balogh).

0191-8141/$ - see front matter © 2007 Elsevier Ltd. All rights reserved.
doi:10.1016/j.jsg.2007.10.007

microfabric studies alone may be insufficient to resolve this problem, and additional data are required for the adequate evaluation.

The effects of shear strain on (very) low-T metamorphic tectonites were studied mostly in context with phyllosilicate characteristics (i.e. illite and chlorite "crystallinity" indices, mean crystallite thickness, lattice strain), as well as vitrinite reflectance in the past decades (see e.g. Teichmüller et al., 1979; Roberts and Merriman, 1985; Frey, 1987; Kisch, 1989; McCaig and Knipe, 1990; Merriman et al., 1990, 1995; Roberts et al., 1991; Warr et al., 1996; Árkai et al., 1997, 2002; Merriman and Peacor, 1999; Giorgetti et al., 2000; Burkhard and Badertscher, 2001; Burkhard and Goy-Eggenberger, 2001; Abad et al., 2003; Carosi et al., 2003). The (sometimes controversial) results of these works suggest that the response of phyllosilicates to increasing strain depends on numerous physical and chemical factors during and following deformation and (re)crystallization. Therefore, careful studies using an integrated, multidisciplinary approach are of crucial importance in the better understanding and correct interpretation of (very) low-grade fault rocks.

The present work provides such a complex case study on a transitional, brittle–ductile shear zone developed in the Middle Triassic, low-T metavolcanic sequence of the Eastern Bükk Mountains (NE Hungary), whereas a combination of microstructural, petrological and geochronological methods was used in order to characterize the type, age and factors controlling the formation and evolution of this shear zone.

2. Geological and structural setting

The rocks studied in this work originated from the Bükk Unit, i.e. the innermost tectonic unit of the Gemer-Bükk region of the Western Carpathians in Central Europe (Fig. 1B). The Bükk Unit comprises Late Paleozoic and Mesozoic sequences formed originally at the southern margin of the Neotethyan oceanic branch, in the presumable paleogeographic neighbourhood of South Alpine–Inner Dinaridic units (e.g. Kovács et al., 2000; Filipović et al., 2003).

The Bükk Unit can be divided into two major tectonic units formed during Upper Jurassic(?)–Early Cretaceous nappe stacking (Csontos, 1988, 1999, 2000; Fig. 1A): (1) the lower "Bükk Parautochthon", built up by Middle Carboniferous–Middle to Late(?) Jurassic sequences; (2) the overlying Szarvaskő-type nappes, consisting of Jurassic basic magmatites and/or associated siliciclastic and carbonate rocks. This primary nappe structure was folded into map-scale, roughly E–W trending, gently to moderately inclined, south-vergent F_2 folds (Fig. 1A), associated with a regional, northward-dipping, S_2 (axial plane) foliation (Schréter, 1943; Balogh, 1964; Csontos, 1988, 1999). These major F_2 structures were later refolded in several phases (Csontos, 1988, 1999; Fodor, 1989). The ages of the penetrative F_2 and the subsequent, less important (F_3–F_4) folding phases were placed into the late Early Cretaceous (Barremian–Albian?; Csontos, 1999). Nappe stacking and early F_2 folding were associated with a regional, low-T metamorphic imprint (Árkai, 1973,1983; Árkai et al., 1995a), displaying a remarkable spatial variability (from deep diagenesis to almost epizonal[1] conditions; Fig. 1A). Using white K-mica K-Ar isotopic and zircon fission track data the Alpine regional metamorphism was dated between 140 and 110 Ma in the largest part of the Bükk Mts. (Árkai et al., 1995a; Fig. 1A).

The eastern part of the mountains, forming the study area of this work (Fig. 1A), exposes the Bükk Parautochthon, i.e. the lower tectonic unit. The section studied in a road-cut at the resort place Lillafüred (Figs. 2A and 3A) represents the northernmost segment of the Middle Triassic (Anisian/Ladinian) stratovolcanic sequence called Szentistvánhegy Metaandesite Formation (Haas, 1995; Less et al., 2002; Pelikán et al., 2005), comprising predominantly fine-grained, pyroclastic rocks and lavas mostly of andesitic, dacitic and rhyolitic compositions (Szentpétery, 1929, 1932, 1935, 1936; Pantó, 1951, 1961; Balogh, 1964; Szoldán, 1990). These rocks experienced high-T anchizonal to epizonal (greenschist facies chlorite zone) metamorphism (Árkai and Sadek Ghabrial, 1997; Árkai et al., 2000; Mata et al., 2001). Although signs explicitly proving the volcanoclastic origin (e.g. lapilli, pumices, rock and crystal fragments) are lacking in the rocks studied, the well-developed penetrative cleavage and banding suggest fine-grained, tuffaceous origin, as lava rocks of the investigated sequence are generally massive and fractured, containing fissure fillings connected to regional metamorphism.

Concordant white K-mica K-Ar and zircon fission track ages between 77 and 98 Ma in the Eastern Bükk (Árkai et al., 1995a; Fig. 1A) showed that temperatures exceeding 200 °C also existed here during a relatively young phase of the Eoalpine cycle. The sharp deviation of the radiometric ages here from other parts of the Parautochthon unit could be interpreted either by regional differences in the cooling history of this unit or by Late Cretaceous semi-ductile deformation along a ca. NW–SE striking shear zone, known as "Bükkszentkereszt Fault" (Csontos, 1988, 1999; Fig. 1A).

Structurally, the Szentistvánhegy Metaandesite is situated at Lillafüred in the southern limb of a major F_2 antiform anticline termed as "North Bükk anticline" (Balogh, 1964; Csontos, 1988; see Fig. 1A). The metavolcanic series forms here a 200–250 m thick (real thickness), moderately to steeply NNE-dipping horizon between shallow-water, Triassic carbonates with the same dip (Fig. 2A). The northern contact of the metavolcanite series with the stratigraphically underlying Anisian Hámor Dolomite is covered by scree on the steep, eastern slope of the Szentistván-hill in the studied profile (Fig. 3A,E). In the south, the metavolcanite stripe is bounded by the stratigraphically overlying Ladinian Fehérkő Limestone (not exposed in the section studied). Bedding-cleavage relationship and southward younging biostratigraphic data (Balogh, 1964, 1981; Haas, 1995; Velledits, 1999) indicates consistently the overturned position of these lithological units (Fig. 2A,B).

At the contact of the metavolcanite with the Hámor Dolomite, a heavily sheared zone is developed parallel to the

[1] The terms "anchi- and epizones" are used in context with illite "crystallinity" (Kübler index) data as determined by Kübler (1968, 1990).

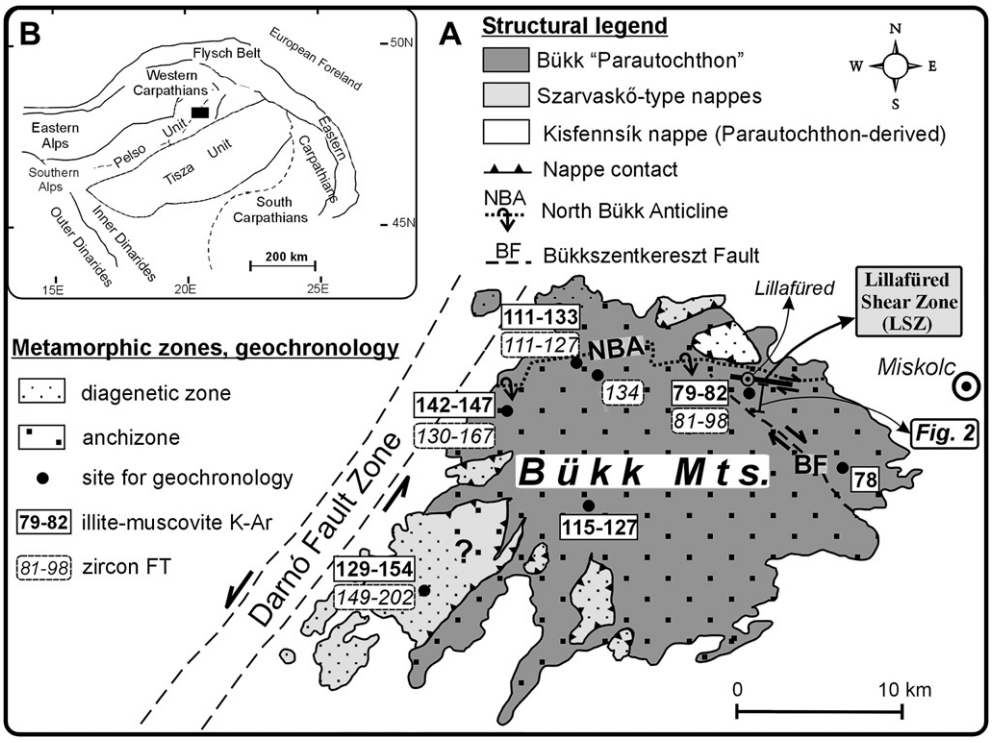

Fig. 1. (A) Schematic pre-Tertiary geological map of the Bükk Mts. (modified after Csontos, 1988) showing the major tectonic units, the rough distribution of Cretaceous metamorphic conditions, and also available geochronological data after Árkai et al. (1995). (B) Inset shows the location of the Bükk Mts. (black rectangle) within the Alp-Carpathian-Dinaridic frame.

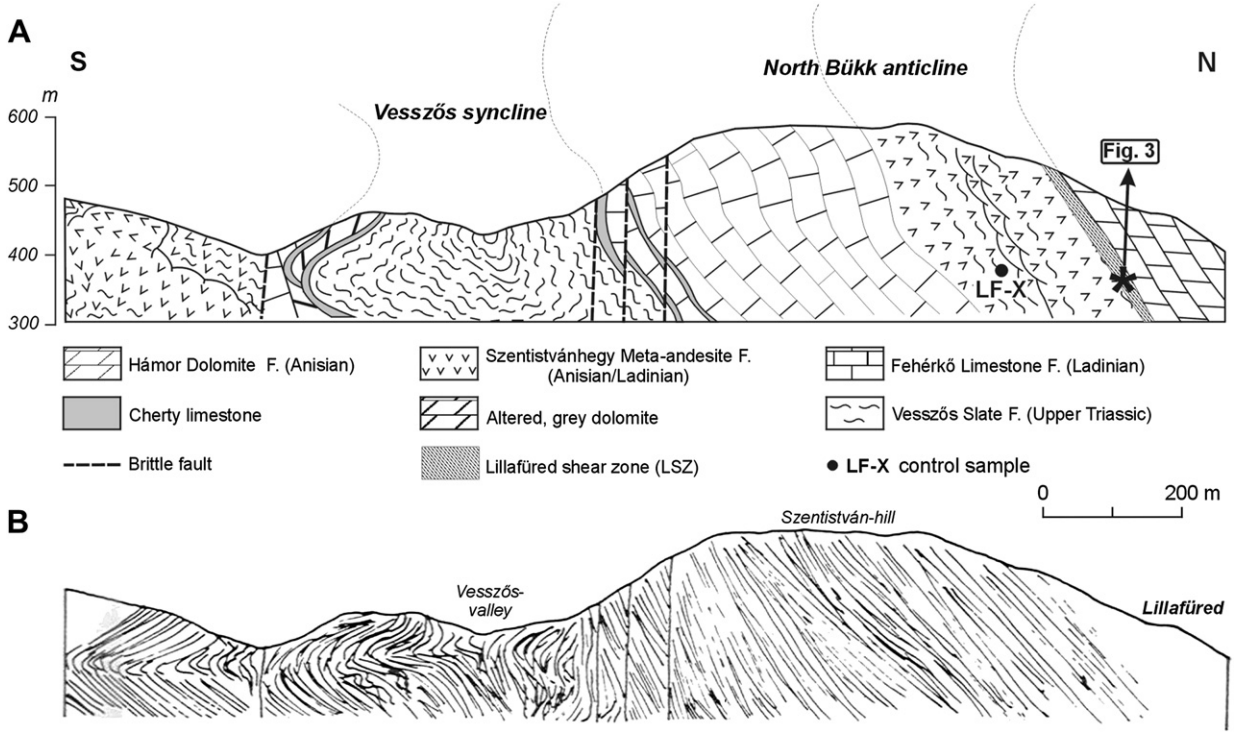

Fig. 2. (A) Geological profile (position shown in Fig. 1A) in the western side of the Szinva valley (slightly modified after Csontos, 1999). Note the southward younging stratigraphic relationships indicating the overturned position of the southern limb of the ''North Bükk anticline''. Location of the studied section (Fig. 3) and the control sample LF-X are also indicated. (B) Position of the regional S_2 foliation formed as axial plane foliation during F_2 folding along the same profile. Note that in the north bedding dips more steeply to NNE than S_2 indicating overturned position. Late F_3 folding is pronounced in the middle part (''Vesszős syncline'') of the profile (after Csontos, 1999).

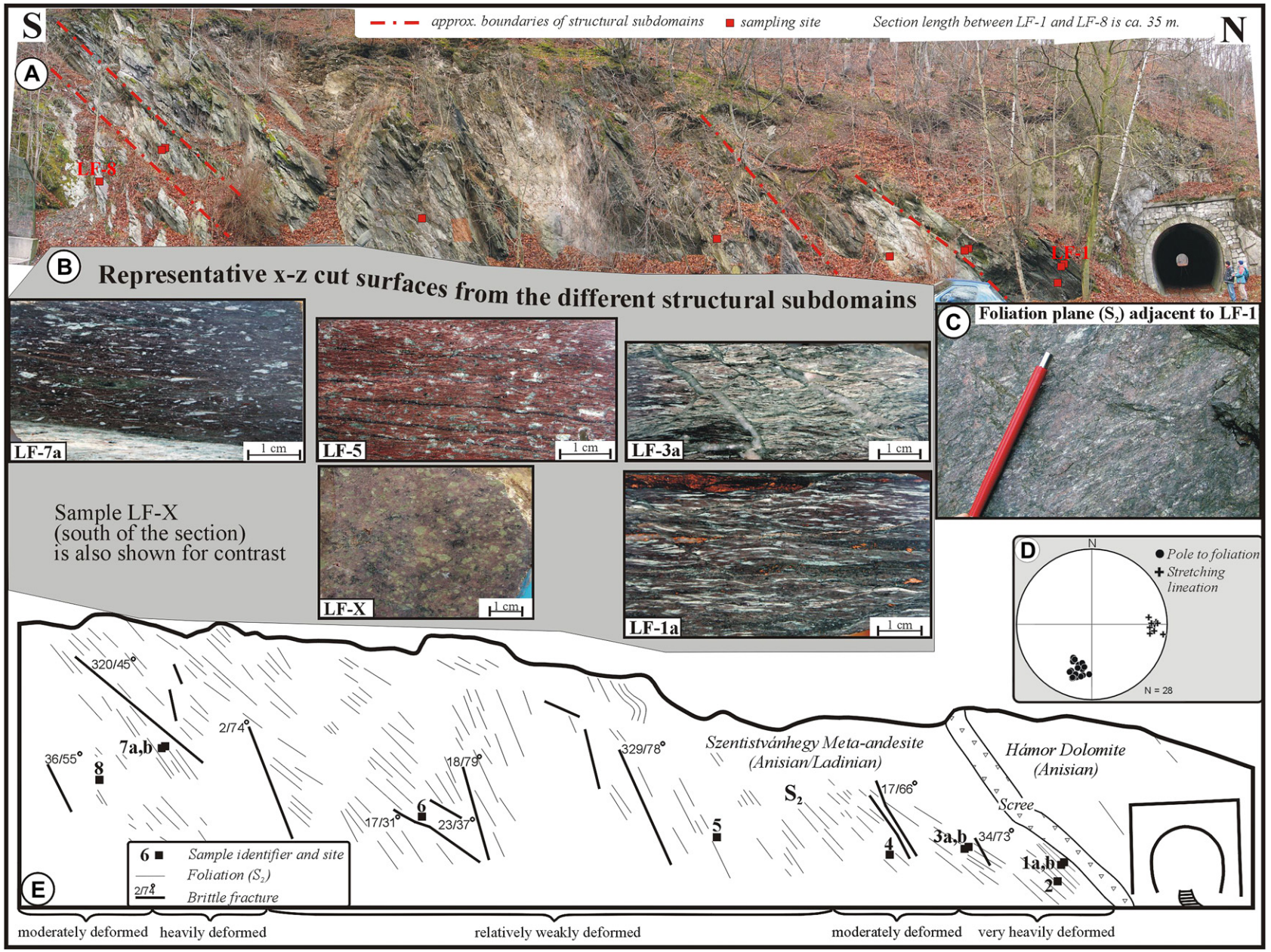

Fig. 3. (A) Photomontage of the detailed section of the Szentistvánhegy Meta-andesite Formation at Lillafüred. (B) Contrasting fabrics on polished cut surfaces from the weakly (LF-5) and heavily deformed (LF-1, -3, -7) structural subdomains. (C) Whitish, elongated feldspar porphyroclasts in the foliation (X–Y) plane defining a gently eastward plunging stretching lineation at the northern end of the section. (D) Measured foliation (S_2) and stretching lineation (L) data in the section (equal area, lower hemisphere projection). (E) Line drawing of the section showing characteristic structural features and sample sites as well.

regional S_2 foliation (Fig. 2A), expressed by the localized appearance of well-foliated and lineated, macroscopically mylonite-like rocks. This zone—called further on the Lillafüred Shear Zone (LSZ)—was studied in detail along a ca. 35 m long, N–S oriented section (Fig. 3) at the western slope of the Szinva valley, and compared to its wider surroundings in order to decipher the relationship between the intensity of strain and the various metamorphic petrological parameters, as well as the geochronological data, furthermore to constrain the role and possible interactions of the factors controlling the formation and evolution of the LSZ.

3. Results

3.1. Structural features

3.1.1. Outcrop-scale observations

At outcrop-scale a closely-spaced (millimetre-scale), penetrative foliation (S_2, Fig. 3A,E) dipping moderately to the NNE (in average: 20/55°) is the most characteristic structural feature of the brownish purple-green metatuff series. Primary magmatic features are not to be recognized any longer. Locally, the penetrative foliation is slightly folded into small-scale (maximum several dm), open to close, sometimes kink-like F_3 folds with ca. ESE–WNW trending fold axes. In contrast, no or only very weakly-developed foliation was observed in the Hámor Dolomite at the northern end of the section. Moderately to steeply NNE-dipping fractures subparallel to the dominant S_2 foliation and less common N- to NW-dipping joints (Fig. 3E) were formed during late-stage brittle deformation.

Based on various macroscopic criteria (e.g. development of the foliation and stretching lineation, strain intensity in mineral-aggregates; see Table 1) several subdomains could be distinguished in the section (Fig. 3A,E). The northernmost, highly strained subdomain is characterized by a well-developed, subhorizontal to gently eastward plunging stretching lineation defined by the alignment of lath-shaped, whitish, altered feldspars and elongated, dark greenish chlorite patches formed after magmatic mafic minerals (Fig. 3C,D). Cut surfaces parallel to the stretching lineation and perpendicular to the foliation (i.e. the X–Z fabric plane) display here ultramylonitic[2] rock fabrics at hand-specimen scale with highly strained mineral-lenses (LF-1a,b and -3a,b; Fig. 3B). Conjugate sets of shear bands are very characteristic here, often accompanied by 0.2–8 mm thick, (sub)parallel calcite (±quartz) veins (Fig. 3B). The conjugate sets are unequally developed and distributed throughout the whole rock volume, indicating virtually opposite sense of shear in the adjacent, smaller (several cm-scaled) rock domains. However, most shear bands—which form locally also an incipient extensional crenulation cleavage—indicate top-to-the-E shear along the NNE-dipping foliation.

The next subdomain to the south shows moderate deformation (cf. Table 1). In sample LF-4 only one set of shear bands is present, indicating top-to-the-E shear.

In the middle part of the section, the investigated rocks are still well-foliated (samples LF-5,-6), but the stretching lineation—showing the same, gently eastward plunging orientation (Fig. 3D)—is much less prominent, or locally even not recognizable. Shear bands are missing. Axial ratios of deformed mineral(aggregate)s in the X–Z plane are also the least here in the section (Table 1, Fig. 3B).

Near the southern end of the section, deformation was more intensive as expressed both by the better developed (more closely spaced) foliation and stretching lineation (samples LF-7a,b and -8). Samples LF-7a and b contain again relatively highly strained mineral lenses in the X–Z plane (Fig. 3B). Furthermore, weakly-developed shear bands also appear here, indicating top-to-the-E shear.

Finally, the sample LF-X, collected for control purposes ca. 200 m south of the studied section (Fig. 2A), shows macroscopically no intense deformation as indicated by the weakly-developed foliation without any stretching lineation.

3.1.2. Microfabrics

For detailed microstructural investigations oriented samples were collected from the outcrop-scale structural subdomains displaying different intensity of deformation (Fig. 3E). Oriented thin sections (at last two pieces from each sample) were prepared from rock slabs cut parallel to the X–Z fabric plane.

All samples deriving from the LSZ display an excellently developed, (domainal) spaced foliation (Fig. 4A,B,E–G), defined by the alternation of slightly anastomosing phyllosilicate-rich (white mica, chlorite, ±calcite) and relatively feldspar-(±quartz)-rich bands and/or lenses. Fine-grained, phyllosilicate-rich domains, recrystallized from the original magmatic groundmass, are characterized internally by a continuous foliation. Primary magmatic mineral phases and features are not observed. In contrast, the control sample LF-X displays an internally weakly deformed microstructure without a clearly defined foliation (Fig. 4I), whereas original magmatic fabric is locally well-preserved.

Original feldspar phenocrysts or phenoclasts—which were totally albitized during metamorphism—form mostly angular porphyroclasts of 0.1–10 mm, winged frequently by asymmetric tails of the matrix minerals (Fig. 5A). Feldspars are strongly cracked in all samples and almost totally altered into heavily elongated, white mica-dominated, fine-grained aggregates in the most highly strained samples (LF-1ab, -3ab, -7ab; Fig. 4A,B,F). These are extremely elongated, whitish lenses on the macroscopic scale (Fig. 3B). Feldspar porphyroclasts are often cut by fairly regular sets of syn- and antithetic microfaults (Figs. 4E and 5C), along which mm-scaled displacement is not uncommon in the moderately and highly strained rocks (LF-1ab, -3ab, -4, -7ab, -8), whereas only minor offset occurs between the individual fragments in the least deformed samples (LF-5, -6). The antithetic fracture set appears preferentially in moderately deformed samples (LF-4, -8), frequently forming

[2] The terms ultramylonitic, mylonitic, etc. are used here strictly for the phenomenological description of the characteristic macroscopic appearance of the studied fault rocks (i.e. well-foliated rock with associated stretching lineation, shear sense indicators and ductile-deformed mineral-aggregates).

Table 1
Overview on the most important (micro)structural features of the oriented samples

Sample	Distance from the northern end of the section (m)	Foliation (S)	Intensity of the foliation	Stretching lineation (L)	Intensity of the stretching lineation	Proportion of rigid, unaltered porphyroclasts and macroscopic rock structure	Strain-magnitude in XZ plane (max. axial ratios of elongated aggregates)	Extent of feldspar alteration	Shear sense indicators	Shear sense	Remarks
LF-1a	0.1	18/47	Excellent, very closely spaced	90/18	Well-developed	<10−15% "ultramylonitic"	High (up to 1:10−20)	Very intense, (almost total)	Shear bands (locally: ECC), σ-clasts, syn- and antithetically sheared feldspar-fragments	Dextral strike-slip	Conjugate sets of shear bands
LF-1b	0.2	10/53	Excellent, very closely spaced	88/16	Well-developed	<10−15% ultramylonitic	High (up to 1:10−20)	Very intense, (almost total)	Shear bands, σ-clasts, syn- and antithetically sheared feldspar-fragments	Dextral strike-slip	Conjugate sets of shear bands
LF-2	0.5	–	–	–	–	–	–	–	–	–	Unoriented sample for petrology-geochronology, fabric as in LF-1 and -3
LF-3a	1.7	14/44	Excellent, very closely spaced	89/14	Well-developed	<15% ultramylonitic	High (up to 1:10−20)	Very intense, (almost total)	Shear bands	Sinistral? strike-slip	Conjugate sets of shear bands
LF-3b	1.75	14/44	Excellent, very closely spaced	89/14	Well-developed	<15% ultramylonitic	High (up to 1:10−20)	Very intense, (almost total)	Shear bands, exceptionally intrafolial folds	Dextral strike-slip	Equally developed conjugate sets of shear bands
LF-4	3.7	12/51	Excellent, very closely spaced	98/5	Weakly-developed	25−45% mylonitic	Low (max. 1:2−4)	Moderate, although strongly cracked and boudinaged	Weakly-developed shear bands, σ-clasts, "domino-structure"	Dextral strike-slip	Abundant fibrous calcite between rigid feldspar-fragments, microstructure, protolith as in LF-8
LF-5	9.4	20/65	Good, closely spaced	99/23	Very weakly-developed (hardly observable)	35−55% protomylonitic	Low (max. 1:4)	Moderate (∼least), although strongly cracked	"Domino"-structure, in small domains: weakly-developed S-C structure	Dextral strike-slip	Only few fibrous calcite between rigid feldspar-fragments, microstructure, protolith as in LF-6
LF-6	23.4	16/62	Good, closely spaced	96/18	Weakly-developed	20−40% protomylonitic	Low (max. 1:4)	Moderate, although strongly cracked	Not observed	–	Only few fibrous calcite between rigid feldspar-fragments
LF-7a-b	32.4−32.45	10/58	Excellent, very closely spaced	83/25	Moderately-developed	<10% ultramylonitic	Moderate (up to 1:10)	(Almost) totally altered into white mica	Weak shear bands, in small domains: S-C structure	Dextral strike-slip	Only few fibrous calcite between rigid feldspar-fragments
LF-8	35.0	12/60	Excellent, very closely spaced	89/22	Weakly-developed	25−40% mylonitic	Low−moderate (up to 1:5−6)	Moderate, although strongly cracked and boudinaged	Weakly-developed shear bands, σ-clasts, "domino"-structure	Dextral strike-slip	Abundant fibrous calcite between rigid feldspar-fragments
LF-X	∼200	–	Weakly developed	–	Not developed	30−40% weakly deformed	Negligible	Moderate	–	–	Unoriented control sample for petrology-geochronology ca. 200 m south from the LSZ

Data of two unoriented samples (LF-2 and LF-X) collected for petrological and geochronological control purposes within and outside the LSZ are also shown.

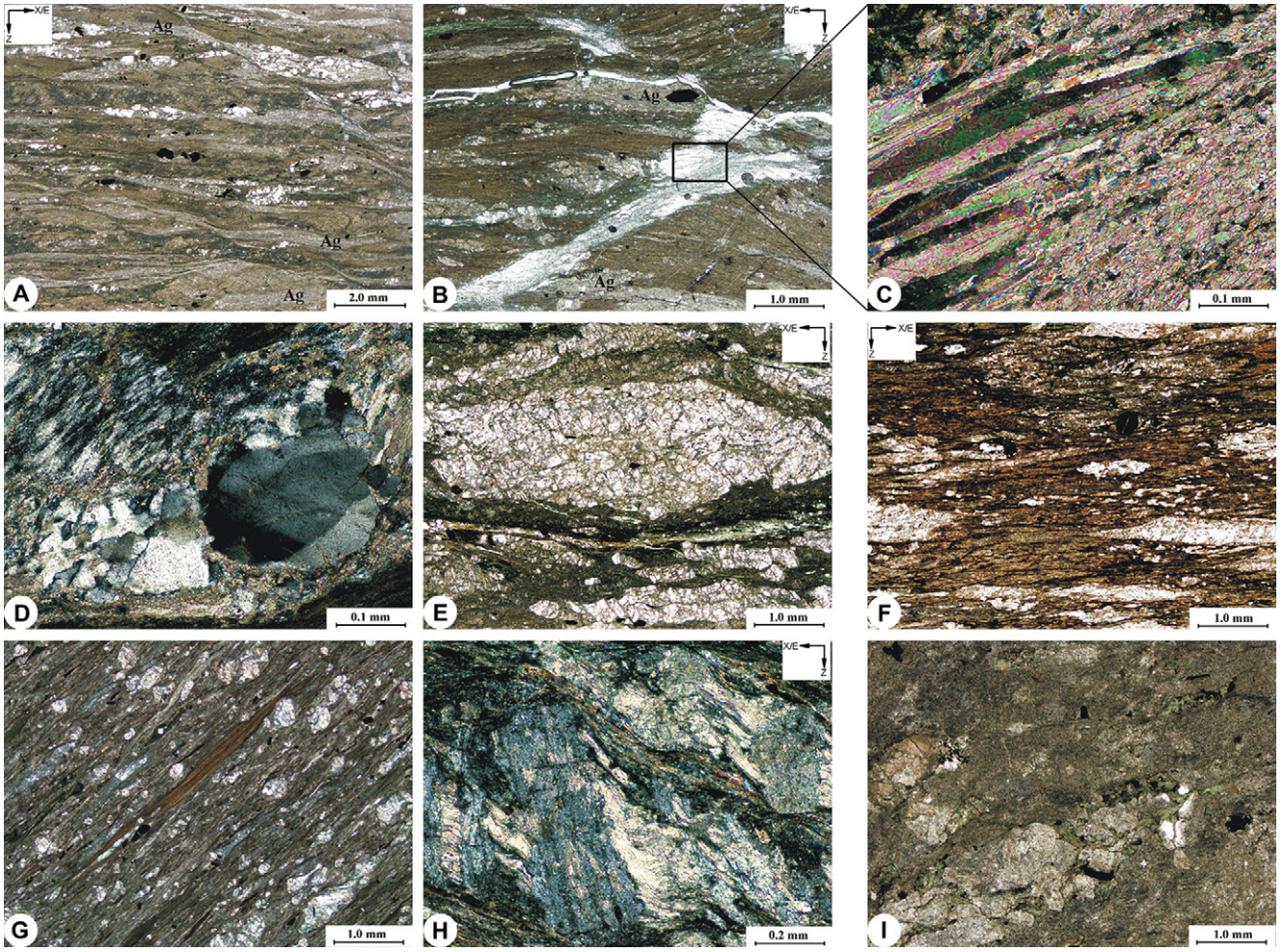

Fig. 4. Representative microfabrics from the LSZ. (A) Ultramylonitic rock structure with a single, well-developed set of shear bands indicating dextral shear sense. Note also heavily elongated, fine-grained, lighter micaceous aggregates (Ag, also in B) after feldspar. LF-1a, 1N. (B) Ultramylonitic fabric with conjugate sets of shear bands along which syntectonic calcite (white) was grown. Rectangle shows the position of (C). LF-3a, 1N. (C) Microfabric detail enlarged from (B). Elongated, thin crystals of 3b fibrous calcite (left) grown syntectonically along a shear band. Fibrous grains pass laterally into a fine-grained, dynamically recrystallized aggregate (right) resulting from continued deformation along the shear band. LF-3a, +N. (D) Two morphological types of quartz: (1) fibrous, fine-grained aggregates with poorly defined grain boundaries (upper left); (2) larger grains with undulous extinction, subgrains and minor ''bulging'' recrystallization (lower left). LF-3a, +N. (E) ''Protomylonitic'' fabric with elongate feldspar porphyroclast cut by syn- and prevailing antithetic (dipping to the right) sets of microfractures with negligible offset along them (''mosaic'' type clast). Sinistral sense of shear. LF-5, 1N. (F) Elongated, fine-grained micaceous aggregates after feldspar (white) in ultramylonitic rock. S-C like asymmetry of the fabric indicates dextral sense of shear. LF-7a, 1N. (G) ''Mylonitic'' microfabric with weakly altered feldspar clasts (white) and large, elongated, altered mica flake (middle). LF-8, 1N. (H) Boudinaged feldspar with slightly curved, fibrous calcite filling the space between the fragments. LF-8,+N. (I) Hardly deformed microfabrics with cracked feldspars and chlorite. Note also the lack of a pronounced foliation. LF-X, 1N.

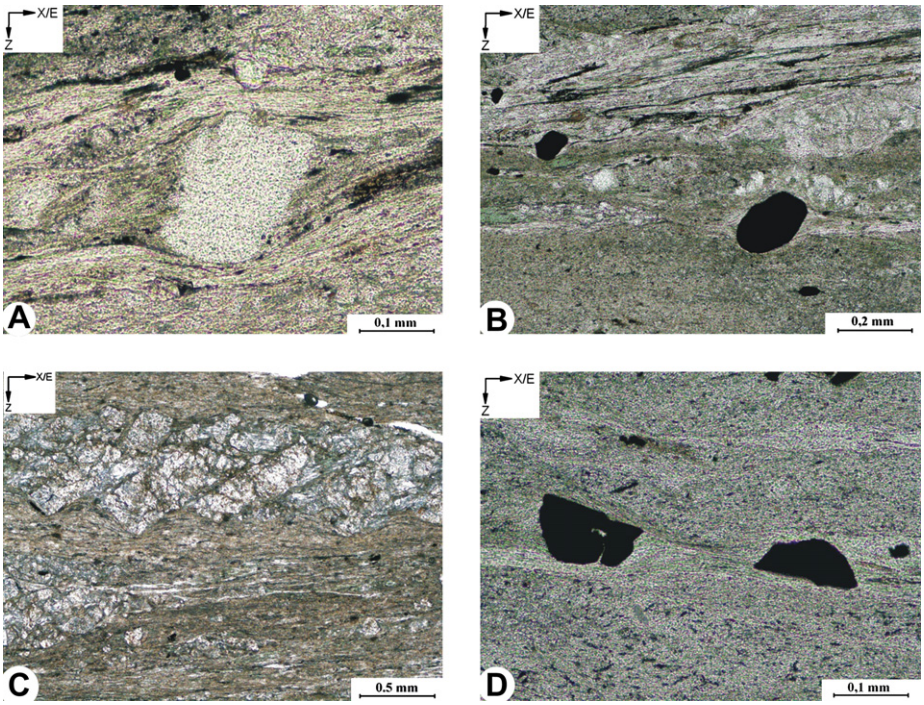

Fig. 5. Shear sense indicators observed in the LSZ. All photos record dextral (top-to-the-E) sense of shear. (A) σ-type feldspar porphyroclast winged asymmetrically by very fine-grained chlorite, white mica and calcite. LF-1a, 1N. (B) Opaque grains with weak stair stepping and asymmetric wings forming σ-type porphyroclasts. LF-1b, 1N. (C) ''Domino''-structure in feldspar grain fragmented by the antithetic fracture set. LF-4, 1N. (D). Opaque grain sheared synthetically along microfracture. LF-1b, 1N.

typical ''domino-structure'' (Fig. 5C). Synthetic shear fractures occur rather in high-strain rocks. Fibrous, slightly curved calcite (±chlorite) subparallel to the finite stretching direction often fills the space between boudinaged fragments (Fig. 4H).

Samples LF-1a and b and especially LF-3a and b contain quartz in considerable amounts (up to 10–15 vol%). It occurs generally in variably elongate, oval-shaped aggregates of 0.5–15 mm aligned parallel to the foliation. These—frequently fractured—aggregates are built up by two morphological types of quartz (Fig. 4D): (1) either purely fine-grained (<0.05 mm), fibrous quartz with poorly-defined, diffuse grain boundaries, or (2) smaller (0.3–3 mm) equidimensional to slightly elongated aggregates of quartz with polygonal or interlobate grain boundaries, which occur rarely in type 1 quartz-aggregates. The individual grains in type 2 quartz are of 0.1 and 0.5 mm, and often show undulous to patchy extinction, rarely subgrains occur as well. Incipient dynamic recrystallization at the grain boundaries by slow grain boundary migration (''bulging'', cf. Stipp et al., 2002) takes place only sporadically. In rare cases, relatively coarse-grained (0.2–1 mm) quartz characterized by polygonal grain boundaries, undulous or patchy extinction and rare subgrains appears also as vein-filling mineral in association with calcite.

White mica and chlorite in the fine-grained matrix show excellently developed preferred orientation. In mica-rich domains perfectly aligned, very small (<0.05 mm) individual flakes form heavily elongate aggregates and lenses, or absolutely continuous stripes with a thickness of 0.5–5 mm. Occasionally larger (0.1–2 mm), elongated, individual mica flakes parallel to the foliation occur as well (Fig. 4G).

Sporadically occurring primary mafic phenocrysts (pyroxene or amphibole?), winged locally by the matrix minerals, were completely replaced by a fine-grained mixture of chlorite and opaque minerals. Furthermore, individual opaque minerals (hematite, pyrite, goethite, ilmenite) of variable grain-size (0.1–2 mm)—present in relatively large quantities in most samples—frequently form idioblastic to hypidioblastic, locally winged, or sheared grains (Fig. 5B,D).

Calcite occurs as secondary phase in three microstructural positions: (1) it fills the space between boudinaged mineral fragments as fibrous, curved crystals (Fig. 4H), (2) occurs as extremely fine-grained, penetrative infiltration in the matrix (Fig. 4D), and (3) forms 0.1–5 mm thick veins in the shear band planes, or subparallel to them (Fig. 4B,C). Within the veins, two morphological types of calcite were observed: (3a) either relatively coarse-grained (up to 2 mm), equant calcite with equigranular-polygonal grain boundaries showing intense twinning (type II and III twins; Burkhard, 1993), and/or (3b) heavily elongated, fibrous, slightly curved calcite grains (Fig. 4C). The long axis of (3b) calcite fibres is oriented (sub)parallel to the finite stretching (x) direction, or—less frequently—to the shear band planes. This feature clearly argues for the syntectonic crystal-growth of calcite, indicating also intense fluid migration during shearing. Moreover, sporadically occurring dynamic recrystallization of (3b) fibrous calcite (Fig. 4C) proves continued shearing after syntectonic crystal-growth.

Epidote and clinozoisite occurs in small quantities only in sample LF-X, replacing original mafic minerals (presumably amphibole or pyroxene) in association with chlorite and fine-grained opaque minerals.

3.1.3. Sense of shear

Well-developed shear sense indicators—as shear bands, σ-type clasts, ''domino''- and S-C structure, exceptionally intrafolial folds (Figs. 4A and 5)—are abundant in the heavily deformed rocks, but less frequently they also occur in the less deformed samples (Table 1). Well-developed, conjugate sets of shear bands, observed at micro-scale as well (Fig. 4B), occur exclusively in the most heavily deformed rocks (LF-1ab, -3ab), suggesting that their formation is intimately related to high accommodated bulk-strain, probably at the late stage of progressive deformation (Platt and Vissers, 1980; Passchier, 1984; Platt, 1984).

The sense of shear determined in thin sections was consistent with the macroscopic observations which altogether—with one exception—record top-to-the-E shearing corresponding to dextral strike-slip motion along the NNE-dipping foliation. The only exception is sample LF-3a, where shear bands seem to indicate top-to-the-W transport. As mentioned previously (cf. ''Outcrop-scale observations'') shear band sets are unequally distributed throughout the whole rock volume, and sample LF-3a represents such a situation, where antithetic shear bands (with respect to the top-to-the-E bulk shear) are predominant over the synthetic ones at thin section scale. As there is no other reliable indicator present in this sample, the top-to-the-W transport could not be confirmed. Such a phenomenon (i.e. virtually opposite shear senses in certain rock volumes) is not uncommon in shear zones associated with conjugate sets of shear bands (e.g. Platt and Vissers, 1980; Platt, 1984).

3.1.4. Distribution of strain

Clearly, strain is distributed heterogeneously in the investigated profile as reflected both in macro- and microstructural features (Fig. 3B,E and Table 1). Generally, the deformation pattern is characterized by the alternation of narrow, high-strain and wider, low-strain domains. The majority of the displacement was concentrated obviously into the narrow (several dm wide), high-strain zones at the northern (samples LF-1ab, -3ab) and near the southern end (LF-7ab) of the LSZ, as indicated by the prominent macroscopic ultramylonitic rock structure with well-developed shear sense indicators. Other parts of the section were affected by a considerably less intense shearing, as reflected in the mylonitic (LF-4 and -8) and protomylonitic (LF-5 and -6) fabrics and the lack of well-developed stretching lineation. Weak to moderate alteration of feldspar and the lack (or negligible amount) of fibrous calcite between the boudinaged mineral fragments in the least deformed subdomain (LF-5, -6) clearly points to the crucial role of fluids in strain partitioning within the LSZ.

It must be emphasized that final rock fabrics were also significantly influenced by the primary mineralogical–lithological properties (e.g. the original proportion and distribution of feldspar phenocrysts in the groundmass, average size of phenocrysts, etc.). Sample LF-6, for example, shows the same (or even lower) proportion of porphyroclasts as samples LF-4 and -8, although in other respects (as the presence of well-developed shear sense indicators, the amount of displacement of boudinaged feldspar-fragments) it is definitely less deformed than the other two samples.

3.1.5. Grain-scale deformation mechanisms

Rigid porphyroclasts (weakly and unaltered feldspar, opaque minerals) record exclusively brittle behaviour as shown by the frequent syn- and antithetic microfaults in these minerals (Figs. 4E and 5C,D). Activity of pressure solution is indicated by irregularly spaced, dark brown to blackish, anastomosing solution seams in the fine-grained, phyllosilicate-rich matrix (Fig. 4G), truncating locally feldspar porphyroclasts. Solution mass transfer is also clearly evidenced by the widespread fibrous overgrowths consisting of white mica and chlorite (±calcite) in strain shadows around porphyroclasts (Fig. 5A,B).

Subordinate amount of intracrystalline deformation was observed only in the most heavily deformed samples (LF-1ab, -3ab). Low-strain deformation microstructures (undulous extinction, subgrains) and incipient ''bulging'' recrystallization in quartz indicate only very limited dislocation glide. Dynamic recrystallization of vein-filling, fibrous calcite (type 3b) into fine-grained aggregates along shear bands took place only sporadically. Consequently, crystalplastic deformation had only a negligible role in the accommodation of the total strain within the LSZ. Considering the above microstructures, as well as the occurrence of type II and III e-twins in vein-filling, coarse-grained, equant calcite, deformation temperature not exceeding 250–270 °C can be roughly estimated (cf. Burkhard, 1993; Stipp et al., 2002).

The extremely fine grain-size of the phyllosilicate-rich matrix makes the identification of other active deformation mechanisms very difficult. However, the excellent preferred orientation within the phyllosilicate-rich layers suggests that—besides re- and/or neocrystallization related basically to the peak of the metamorphic evolution—passive mechanical rotation of the individual grains occurred as well. Furthermore, intergranular sliding within the phyllosilicate-rich layers and aggregates is of basic importance, too, that is indicated by the recorded very high finite strains of phyllosilicate-dominated aggregates replacing fractured feldspars (LF-1ab,-3ab,-7ab; Fig. 4A,B), compared to the samples with only minor to moderate alteration of feldspars (cf. Fig. 3B and Table 1).

How far the intergranular sliding within phyllosilicate-rich matrix was frictional or viscous is difficult to assess purely on the basis of microstructural observations, which makes also the classification of the studied fault rocks somewhat problematic using the (genetic) criteria suggested by Schmid and Handy (1991). Regarding the microstructures indicative of fluid-assisted solution creep (fibrous overgrowths, solution seams) and the very high finite strains, viscous grain boundary sliding (VGBS) was most probably active in the most heavily sheared rocks (mylonites). In the less deformed samples, the role of VGBS seems to be subordinate. In any case, stable (frictional) sliding (''ductile''[3] granular flow) was certainly

[3] The term ''ductile'' is used here and further on in a non-mechanistic, purely phenomenological sense.

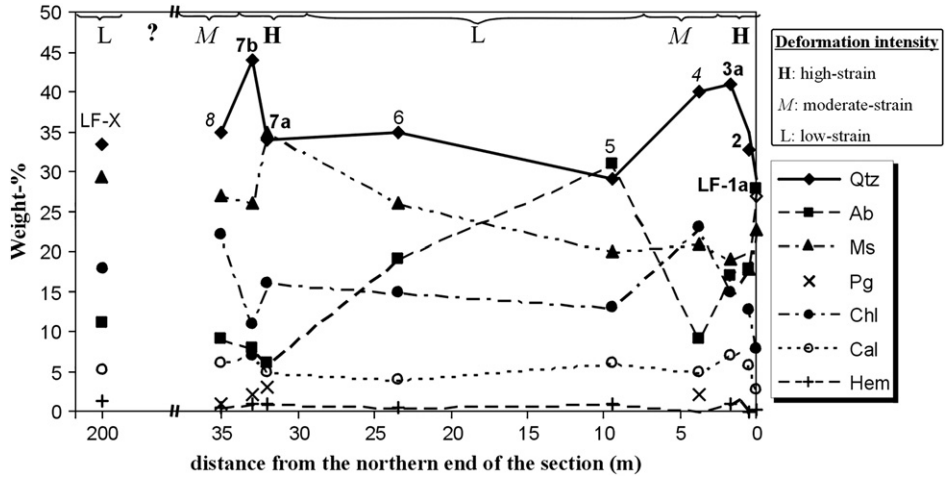

Fig. 6. Variations in semi-quantitative modal composition along the studied profile. For instrumental details and sample preparation techniques see Árkai et al. (2000).

achieved also in these rocks, as suggested by their ''ordered'', mylonite-like appearance (foliated cataclasites). Recent experimental studies (Bos and Spiers, 2001; Bos et al., 2001) have shown that ''classical'' mylonitic rock structure can be formed in fine-grained, phyllosilicate-rich rock analogues (halite–kaolinite mixture) deformed at room temperature by combined cataclasis and pressure solution accommodated intergranular sliding, whereas a frictional-viscous behaviour was observed at high strains of the progressive deformation. These results imply that similar grains-scale deformation processes may also operate in phyllosilicate-rich, transitional brittle–ductile, crustal fault rocks characterized by (very) low-T conditions. Considering the observed microstructural features, we suggest basically a similar deformation regime responsible for the genesis of the mylonitic fault rocks of the LSZ.

3.2. Petrological and mineralogical features

3.2.1. Modal and bulk chemical compositions

Semiquantitative modal compositions of the studied samples (Fig. 6) were determined by X-ray powder diffractometric (XRPD) method. Considering the whole rock samples, quartz, white K-mica (muscovite), chlorite, albite, calcite and hematite are the main rock-forming minerals, in decreasing order of quantities. In addition to white K-mica, four samples contain also discrete paragonite phase in subordinate quantities. White K-mica and chlorite are the main constituents of the <2 μm grain-size fraction samples, which also contain subordinate amounts of quartz, albite, occasionally paragonite and hematite. Negligible amounts of smectite also occur. Fairly similar modal composition characteristics were detected in the sample LF-X outside the LSZ.

Bulk chemistries (Table 2) refer to mostly andesitic, partly dacitic primary magmatic compositions. It must be emphasized, however, that pervasive metamorphism and related fluid migration might modify considerably the bulk compositions.

3.2.2. Phyllosilicate characteristics

XRPD investigations were also carried out on all samples in order to determine metamorphic zones using the illite Kübler index (KI) and chlorite ''crystallinity'' indices (for definitions and description of the method see Kübler, 1968, 1990; Árkai, 1991; Árkai et al., 1995b). There are no systematic and significant differences between the FWHM (full-width-at-half-maximum) values measured on air-dried and glycolated mounts either for white K-mica or for chlorite, implying that there may be minimal amounts of swelling mixed-layers in the

Table 2
Major element composition of bulk rock samples (in weight %)

Sample	SiO_2	TiO_2	Al_2O_3	Fe_2O_3	FeO	MnO	MgO	CaO	K_2O	Na_2O	$-H_2O$	$+H_2O$	CO_2	P_2O_5	Total
LF-1a	63.12	0.90	15.15	1.29	3.25	0.07	1.11	2.82	2.47	3.68	0.06	2.71	2.42	0.17	99.22
LF-2	60.91	0.90	15.65	1.72	3.16	0.08	1.22	4.08	2.08	2.38	0.16	2.71	3.88	0.15	99.08
LF-3a	64.60	0.78	13.30	0.54	3.96	0.08	1.25	3.87	1.88	2.06	0.12	2.76	3.78	0.12	99.10
LF-4	62.35	1.12	16.82	0.14	4.77	0.06	1.91	2.65	1.95	1.23	0.04	3.55	2.33	0.17	99.09
LF-5	61.73	1.08	15.18	1.15	4.42	0.07	0.97	3.37	1.56	3.91	0.05	2.61	3.02	0.20	99.32
LF-6	64.03	1.28	16.35	0.39	3.97	0.06	0.73	2.59	2.46	2.48	0.03	2.95	1.50	0.21	99.03
LF-7/a	59.18	1.29	18.54	0.48	4.64	0.06	1.41	2.67	3.28	1.25	0.07	3.67	2.28	0.21	99.03
LF-7/b	65.94	1.09	15.17	0.52	1.83	0.06	0.79	3.89	2.36	1.31	0.11	2.37	3.29	0.28	99.01
LF-8	58.81	1.16	17.10	0.29	5.96	0.07	2.06	3.04	2.49	1.37	0.15	3.77	2.63	0.29	99.19

Bulk compositions were determined using a Perkin Elmer 5000 atomic absorption spectrophotometer (AAS), after digestion with lithium metaborate. In addition permanganometric (FeO), gravimetric (SiO_2, TiO_2, H_2O and P_2O_5) and volumetric (CO_2) methods were also applied.

mica and chlorite structures, being under the limit of detection by XRPD.

The KI values of the paragonite-free samples within the LSZ refer to high-T anchizonal metamorphic conditions (Fig. 7A); their average practically corresponds to (considering the error of average) the boundary between the anchi- and epizones. The KI values of the paragonite-bearing samples are systematically larger and thus imply apparently lower grades than the KI values of the paragonite-free samples. The calibrated chlorite ''crystallinity'' indices (and their average) fall also into the high-T part of the anchizone (Fig. 7B). The KI value and chlorite ''crystallinity'' indices of the control sample LF-X also clearly refer to high-T anchizonal metamorphism.

Phyllosilicate crystallite thickness or size, referring to the mean size of crystallites (i.e. domains that coherently scatter X-rays) perpendicular to (001), were obtained using the Voigt method of Langford (1978). The XRPD calculated mean crystallite thickness and lattice strain values of white K-micas and chlorites (Fig. 7C–F) fall mainly into the epizone (cf. Árkai et al., 1996; Merriman and Peacor, 1999). The paragonite-bearing samples show smaller mean crystallite size and larger mean lattice strain values than the paragonite-free samples (Fig. 7C,E), which can be explained by the partial overlap of the first basal reflections of paragonite and white K-mica.

For electron microprobe (EMP) analysis three samples displaying fundamental difference in the intensity of shearing (namely LF-1a vs. LF-5 and -6) were chosen, in order to trace

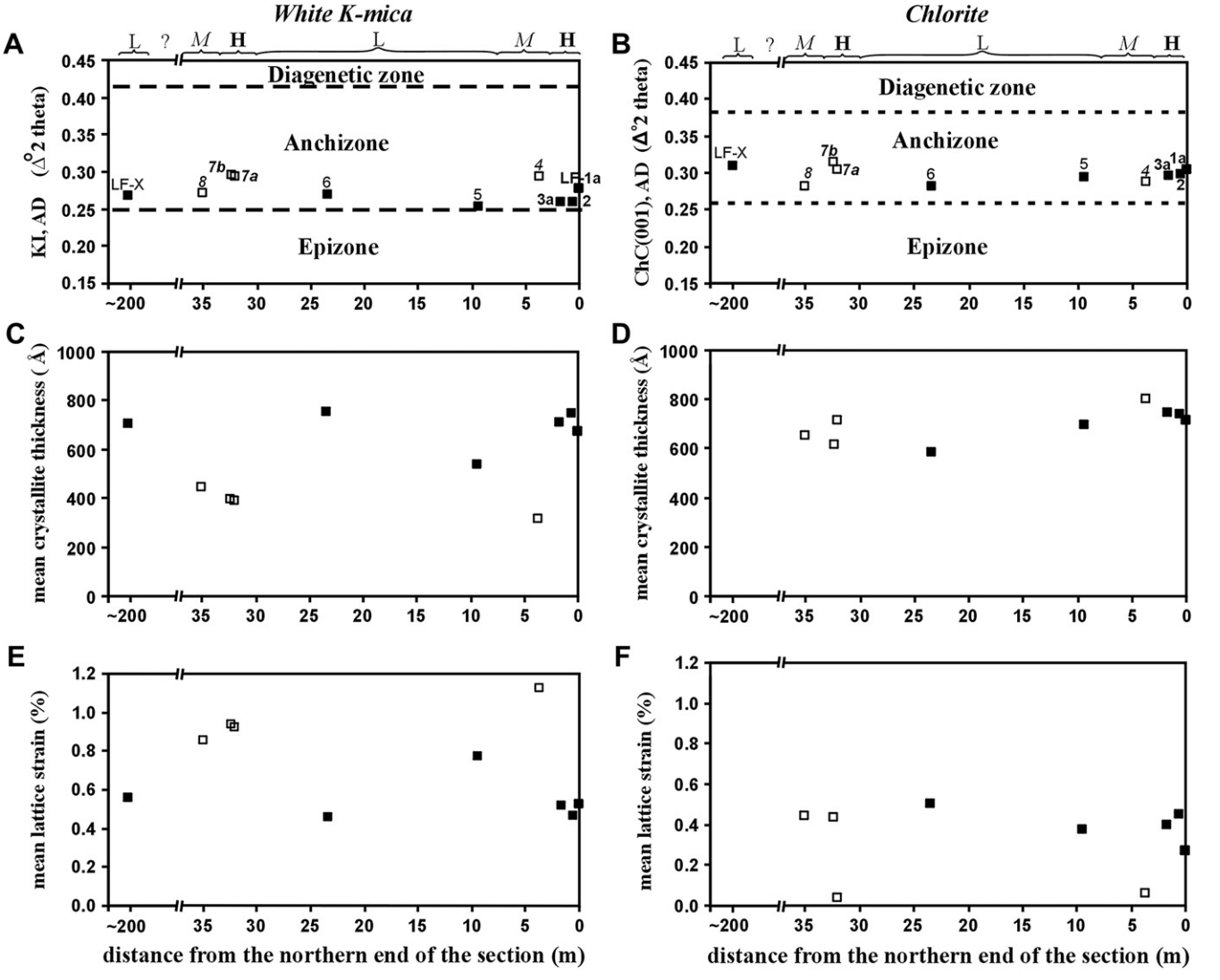

Fig. 7. Variations in illite Kübler index (A) and chlorite ''crystallinity'' index values (B), in apparent mean crystallite thickness (C, D), and lattice strain values (E, F) of the <2 μm grain-size fraction white K-micas and chlorites along the profile. Detailed analytical data with corresponding statistical parameters are available from P. Árkai. For sample preparation techniques, the instrument and methods applied see Árkai et al. (1996, 1997, 2000).

Table 3
Average chemical compositions of white K-micas and chlorites from various microstructural positions in the samples LF-1a, LF-5 and LF-6 (EMP analyses in weight-% and cation numbers)

	White K-mica												Chlorite											
Sample:	LF-1a				LF-5				LF-6				LF-1a				LF-5				LF-6			
Position:	a		b		c		d		e		f		a		b		c		d		e		f	
Statistics:	Mean	Std	Mean	Std	Mean	Std	Mean	Std	Mean	Std	Mean	Std	Mean	Std	Mean	Std	Mean	Std	Mean	Std	Mean	Std	Mean	Std
n	3		3		4		2		5		3		3		3		2		2		4		6	
SiO_2	47.24	0.95	47.24	1.53	45.68	1.27	45.78	1.64	48.13	0.98	49.91	2.63	26.05	0.54	26.55	1.27	24.32	0.13	25.31	0.20	24.23	0.94	24.35	1.12
TiO_2	0.09	0.08	0.09	0.09	0.12	0.11	0.34	0.38	0.14	0.12	0.18	0.16	–	–	–	–	–	–	–	–	–	–	–	–
Al_2O_3	30.38	2.81	31.12	1.46	31.63	1.07	31.46	1.22	30.72	1.36	30.95	1.29	21.02	1.40	20.92	1.35	22.45	0.58	21.56	0.04	19.70	1.08	20.53	1.16
*FeO	3.78	0.86	3.11	0.87	3.91	0.72	3.89	1.13	4.22	0.35	3.76	1.01	25.48	0.46	25.50	0.75	30.93	0.59	30.58	0.57	34.69	0.46	33.31	1.16
MgO	1.46	0.49	1.40	0.31	0.81	0.33	0.86	0.23	0.70	0.18	0.92	0.24	14.96	0.77	13.87	0.44	10.54	0.71	10.91	0.33	7.92	0.72	7.90	0.56
MnO	0.04	0.06	0.04	0.04	0.06	0.07	0.00	0.00	0.08	0.07	0.08	0.13	0.00	0.00	0.00	0.00	0.45	0.11	0.40	0.16	0.24	0.27	0.50	0.36
CaO	0.07	0.06	0.03	0.03	0.21	0.18	0.19	0.06	0.21	0.14	0.00	0.00	0.11	0.07	0.08	0.10	0.05	0.06	0.08	0.11	0.09	0.09	0.08	0.07
Na_2O	0.41	0.18	0.27	0.11	0.80	0.39	1.56	0.62	0.74	0.58	0.84	1.09	0.18	0.08	0.01	0.01	0.12	0.06	0.06	0.08	0.07	0.08	0.11	0.10
K_2O	9.93	0.73	10.62	0.30	8.37	0.65	7.60	0.30	9.47	0.69	9.18	1.48	0.10	0.07	0.18	0.32	0.00	0.00	0.06	0.08	0.06	0.09	0.14	0.13
Total	93.40	1.84	93.93	0.89	91.56	2.22	91.67	0.45	94.39	1.91	95.82	0.15	87.91	1.82	87.10	0.49	88.86	0.81	88.95	0.12	86.98	0.87	86.91	1.65
	Numbers of the cations on the basis of 22 oxygens												Numbers of the cations on the basis of 28 oxygens											
Si	6.48	0.19	6.44	0.15	6.35	0.04	6.34	0.23	6.52	0.13	6.61	0.26	5.47	0.04	5.62	0.27	5.22	0.05	5.41	0.02	5.45	0.15	5.44	0.23
Al^{IV}	1.52	0.19	1.56	0.15	1.65	0.04	1.66	0.23	1.48	0.13	1.39	0.26	2.53	0.04	2.38	0.27	2.78	0.05	2.59	0.02	2.55	0.15	2.56	0.23
Al^t	4.90	0.36	5.00	0.28	5.18	0.13	5.14	0.20	4.91	0.20	4.83	0.25	5.20	0.22	5.22	0.33	5.68	0.07	5.43	0.03	5.22	0.31	5.41	0.27
Al^{VI}	3.38	0.19	3.44	0.13	3.53	0.09	3.48	0.03	3.43	0.09	3.44	0.07	2.68	0.19	2.84	0.16	2.90	0.02	2.83	0.01	2.67	0.18	2.84	0.09
Ti	0.01	0.01	0.01	0.01	0.01	0.01	0.04	0.04	0.01	0.01	0.02	0.02	–	–	–	–	–	–	–	–	–	–	–	–
$*Fe^{2+}$	0.43	0.11	0.35	0.10	0.45	0.09	0.45	0.13	0.48	0.03	0.42	0.12	4.48	0.18	4.51	0.14	5.55	0.18	5.46	0.12	6.53	0.12	6.23	0.23
Mg	0.30	0.11	0.28	0.06	0.17	0.07	0.18	0.05	0.14	0.03	0.18	0.05	4.69	0.25	4.38	0.15	3.37	0.18	3.47	0.09	2.65	0.21	2.63	0.17
Mn	0.00	0.01	0.00	0.00	0.01	0.01	0.00	0.00	0.01	0.01	0.01	0.01	0.00	0.00	0.00	0.00	0.08	0.02	0.07	0.03	0.05	0.05	0.09	0.07
Sum R^{VI}	4.13	0.04	4.09	0.05	4.17	0.08	4.14	0.19	4.07	0.08	4.07	0.12	11.85	0.11	11.73	0.16	11.90	0.04	11.84	0.01	11.89	0.02	11.80	0.11
Ca	0.01	0.01	0.00	0.00	0.03	0.03	0.03	0.01	0.03	0.02	0.00	0.00	0.03	0.02	0.02	0.02	0.01	0.01	0.02	0.03	0.02	0.02	0.02	0.02
Na	0.11	0.05	0.07	0.03	0.21	0.10	0.42	0.17	0.19	0.15	0.21	0.28	0.08	0.03	0.00	0.00	0.05	0.02	0.02	0.03	0.03	0.04	0.05	0.05
K	1.73	0.09	1.85	0.07	1.48	0.12	1.34	0.05	1.64	0.11	1.55	0.27	0.03	0.02	0.05	0.09	0.00	0.00	0.02	0.02	0.02	0.03	0.04	0.04
t.i.c.	1.87	0.05	1.93	0.08	1.76	0.12	1.82	0.20	1.89	0.12	1.77	0.06	0.15	0.06	0.09	0.09	0.07	0.05	0.07	0.00	0.09	0.07	0.12	0.08
Sum(Ca+K+Na)	–	–	–	–	–	–	–	–	–	–	–	–	0.13	0.05	0.07	0.09	0.06	0.04	0.06	0.03	0.07	0.06	0.11	0.07
Total	13.98	0.07	14.01	0.05	13.90	0.03	13.93	0.02	13.93	0.06	13.84	0.15	19.97	0.08	19.80	0.13	19.97	0.00	19.90	0.02	19.96	0.07	19.90	0.12
XMg	0.07	0.03	0.07	0.01	0.04	0.02	0.04	0.01	0.03	0.01	0.04	0.01	0.40	0.02	0.37	0.01	0.28	0.01	0.29	0.01	0.22	0.02	0.22	0.02
$Fe^{2+}/(Fe^{2+}+Mg)$	0.60	0.03	0.55	0.04	0.74	0.05	0.72	0.01	0.78	0.03	0.70	0.04	0.49	0.02	0.51	0.00	0.62	0.02	0.61	0.01	0.71	0.02	0.70	0.02
$Al^{VI}/(Al^{VI}+Fe^{2+}+Mg)$	0.82	0.05	0.84	0.04	0.85	0.03	0.85	0.04	0.85	0.02	0.85	0.04	–	–	–	–	–	–	–	–	–	–	–	–
Na/(Na+K)	0.06	0.03	0.04	0.01	0.13	0.06	0.23	0.06	0.10	0.08	0.12	0.15	–	–	–	–	–	–	–	–	–	–	–	–
Fe^{2+}+Mg	0.73	0.21	0.64	0.15	0.62	0.15	0.63	0.18	0.62	0.07	0.60	0.16	–	–	–	–	–	–	–	–	–	–	–	–
Si/Si+Al^t)	–	–	–	–	–	–	–	–	–	–	–	–	0.51	0.01	0.52	0.03	0.48	0.01	0.50	0.00	0.51	0.02	0.50	0.02
Si+Al^t+Mg+Fe^{2+}	–	–	–	–	–	–	–	–	–	–	–	–	19.85	0.11	19.73	0.16	19.82	0.02	19.77	0.04	19.85	0.04	19.70	0.10
Al^t+Mg+Fe^{2+}	–	–	–	–	–	–	–	–	–	–	–	–	14.37	0.11	14.11	0.40	14.60	0.06	14.36	0.06	14.40	0.13	14.26	0.32

For instrumental details and correction procedures applied see Balen et al. (2006).

Std, standard deviation; *n*, number of measurements; s(x), standard error[=Std/sqr(*n*)]; *Fe, total Fe calculated as FeO or Fe^{2+}; t.i.c., total interlayer charge = Na+K+2Ca. Microstructural positions: a and e = around and in albite porphyroclasts; b, c, d and f = in the foliated matrix.

possible effects of deformation on chemical compositions of phyllosilicates (Table 3). The chemistries of grains found in various microstructural positions were also systematically recorded within each sample.

K-white mica shows fairly uniform composition in the various microstructural positions without any signs of chemical zoning. High FeO (up to 4.2 wt%) and MgO content (0.7–1.5 wt%) is characteristic, the Na_2O content varies between 0.25 and 1.6 wt%. The highest Na_2O values were measured in sample LF-5 which is also the richest in Na_2O according to bulk chemical data (Table 2). Although slight variations exist in analyses from the different samples, no systematic compositional changes could be identified in the context of shear strain. Mineral chemical relations suggest that the Tschermak's type alumino-celadonitic substitution is considerable in white K-mica, while the ferrimuscovitic substitution is negligible. The small but significant deficit in the interlayer charge indicates a combination of alumino-celadonitic and illitic substitutions. Most of the analyses show considerable amounts of Na, which cannot be incorporated in the white K-mica structure at such low temperatures. Consequently, contaminations with intimately intergrown, thin paragonite lamellae may be responsible for this anomaly, even if paragonite could not be detected by XRPD in the samples analysed by EMP.

Chlorite shows mostly Fe-rich composition with XMg [$Mg/(Mg + Fe^{2+} + Al^{VI})$] between 0.2 and 0.4. Similarly to white K-mica, chlorite chemistry is also rather homogeneous within the individual samples. Larger differences exist in FeO and MgO contents between the different samples, but this may reflect the effect of the bulk chemistry control on chlorite compositions, as there is a good correlation between the bulk and chlorite chemical data considering the trends in FeO and MgO (cf. Tables 2 and 3). With increasing differences between Al^{VI} and Al^{IV} (i.e. with increasing deviation from the equilibrium state of the three-three-octahedral chlorites), both the calculated interlayer charge referring to contaminations due to white micas and the apparent octahedral vacancy increase. Consequently, the apparent octahedral vacancy is most probably related to the contaminations by micas measured to the chlorite rather than to an eventual dioctahedral (sudoitic) substitution within the chlorite structure itself.

The metamorphic peak temperature values of the samples analyzed by EMP were calculated using the various calibrations of the empirical chlorite–Al^{IV} geothermometer (Table 4), elaborated originally by Cathelineau and Nieva (1985). Except the calibration of Zang and Fyfe (1995), the various versions gave reliable and consistent results that are in agreement with the estimates based on phyllosilicate "crystallinity" data. Mean temperatures around 350 °C (315–380 °C) correspond fairly well to the boundary realm between the KI anchi- and epizones.

K-Ar age investigations were performed on the white K-mica-rich, <2 μm grain-size fractions. All K-Ar ages from the LSZ vary within a very narrow range (73–77 Ma, in average: 75.8 Ma), and nearly the same age (79 Ma) was found in the weakly deformed control sample LF-X outside the LSZ (Table 5).

Table 4
Peak temperature estimates (°) of metamorphism calculated by the various calibrations of the chlorite-Al^{IV} thermometer

Thermometer	Statistical parameters	Sample		
		LF-1a	LF-5	LF-6
Cathelineau and Nieva (1985)	Mean	333	370	348
	s	31	18	34
	n	6	4	8
	Minimum	277	353	285
	Maximum	365	391	385
Kranidiotis and MacLean (1987)	Mean	315	349	340
	s	20	12	24
	n	6	4	8
	Minimum	278	336	298
	Maximum	337	361	367
Jowett (1991)	Mean	338	379	359
	s	30	18	34
	n	6	4	8
	Minimum	283	361	297
	Maximum	370	399	397
Zang and Fyfe (1995)	Mean	263	277	253
	s	21	11	21
	n	6	4	8
	Minimum	226	267	213
	Maximum	283	291	275

n, number of samples; s, standard deviation.

4. Discussion

4.1. Relationship between the mineralogical–petrological features and the shear strain

Neither the modal composition (Fig. 6), nor the bulk chemical data (Table 2) of the samples show specific trends or changes in function of the intensity of shear strain along the investigated profile, only fluctuations could be demonstrated. The same holds true for the most important metamorphic petrological parameters ("crystallinity" indices, apparent mean crystallite thickness and lattice strain; Fig. 7), as no systematic and significant changes in metamorphic grade (temperature) was observed along the profile, only certain fluctuations (especially in the case of apparent mean crystallite thickness and

Table 5
K-Ar isotopic data of the <2 μm grain-size white K-mica-rich fraction

Sample	K (%)	$^{40}Ar(rad)$ (10^{-5} cm^3/g)	$^{40}Ar(rad)$ (%)	Age (Ma ± 1σ)
LF-1a	4.228	1.295	86.2	77.1 ± 2.9
LF-2	3.721	1.108	79.6	75.0 ± 2.9
LF-3a	3.591	1.101	82.0	77.2 ± 2.9
LF-4	3.036	0.879	76.3	73.0 ± 2.8
LF-5	2.827	0.830	79.7	74.0 ± 2.8
LF-6	4.100	1.248	85.2	76.7 ± 2.9
LF-7a	3.902	1.178	80.3	76.1 ± 2.9
LF-7b	3.365	1.016	78.6	76.0 ± 2.9
LF-8	3.441	1.049	80.0	76.8 ± 2.9
LF-X	4.419	1.390	82.0	79.2 ± 3.0

For details of the method and instruments applied see Odin et al. (1982) and Árkai et al. (1995a), respectively. K-Ar ages were calculated using the constants proposed by Steiger and Jäger (1977).

lattice strain values of white K-mica) were detected. All of the above parameters of the sample LF-X outside the LSZ are very similar to that of the rock mass of the section studied in detail (Fig. 7).

EMP mineral chemical data—disregarding the discussed uncertainties caused by the contaminations/impurities—do not indicate any observable effects of the increasing shear strain on the chemistries of phyllosilicates. Results of the chlorite-Al^{IV} thermometry also indicate fairly homogeneous peak metamorphic temperatures in the samples displaying very different intensity of shearing. Although the most heavily sheared sample LF-1a provided somewhat lower temperature (~330 °C) than the least deformed samples (~350–360 °C), considering also the standard deviations of the mean values, no specific conclusions can be drawn from this difference.

Special attention is paid to the occurrence of paragonite, described for the first time from the Bükk Mts. Since paragonite occurs in moderately sheared samples, it is plausible to suppose that there is no causal relationship between shear deformation and formation of paragonite. A drastic decrease in amounts of albite is observed in those samples which contain paragonite (Fig. 6). This relationship implies that changes in bulk chemistry may be responsible for the occurrence of paragonite.

In summary, neither the different metamorphic petrological parameters nor the mineral chemistries show any evidence for interaction with shear strain in the LSZ. The weakly deformed control sample LF-X at a larger distance from the LSZ and also other metasedimentary rock types in the wider surroundings display practically the same metamorphic conditions (cf. Árkai et al., 1995a). These results imply that the mineralogical-petrological features of the studied rocks were not significantly adjusted during shearing with respect to the enclosing rocks mass.

Traces of phyllosilicate retrogression—including (1) the formation of smectitic and illite/smectite mixed-layers in rims of >500 nm-thick white K-mica crystals formed during the peak metamorphic conditions, and (2) the interstratification of 14-Å chlorite/smectite (corrensite) mixed-layers and 7-Å berthierine layers within large, metamorphic chlorite crystals—were described and interpreted earlier by Árkai et al. (2000) and Mata et al. (2001) in the studied profile. The phenomenon itself was called "retrograde diagenesis" by Nieto et al. (2005), who interpreted this process here as a consequence of Late Cretaceous shearing. The above products of retrogression could be observed mostly only by TEM, therefore they could not basically influence the metamorphic zone-indicating characteristics. Phyllosilicate retrogression—together with the observed microstructural and petrological-mineral chemical features—point to a relatively "cold" and fluid-rich (H_2O, CO_2) regime during shearing.

4.2. Microstructural evolution

In a pure phenomenological approach there exists a strong analogy between the microstructure of the LSZ rocks and "classical" mylonites. Therefore, we will use the terms of mylonite structure described by Handy (1990) in order to characterize microstructures and their evolution in the investigated rocks.

At the early ("protomylonitic") stage of progressive shearing first an IWL_{fv} structure (interconnected weak layer structure with strong clasts of frictional rheology) was formed (samples LF-5, -6), which was basically "predestined" by the precursor tuff-protolith (i.e. fine-grained magmatic groundmass with phenocrysts). Because of the initially low phenocryst/groundmass ratio, a typical load-bearing framework structure (LBF) was probably never realized in the rocks studied, largely enhancing later deformation. It is obvious from the microfabrics observed in the different subdomains of the LSZ that the initial stage was characterized by intense microfracturing of feldspars, which caused important reduction in the average grain-size, and—during progressive deformation—also in the proportion of clasts in the rock matrix. However, grain-size reduction alone could not lead to substantial weakening within the LSZ. Sliding in the phyllosilicate-rich matrix might be also active to some extent, but unambiguous micro- and/or macrostructural evidence for a substantial amount of VGBS is missing in the least deformed structural subdomain.

In the next stage, increasing strain and fluid infiltration (evidenced by syntectonic, secondary fibrous calcite between boudinaged mineral fragments) into the LSZ resulted in the formation of a more pronounced "mylonitic" rock structure (samples LF-4, -8), but the overall structure still shows IWL_{fv} characteristics.

During the last (ultramylonitic) stage, deformation was concentrated into narrow domains, in which the rocks underwent fundamental weakening in consequence of intense retrograde alteration of feldspars into weak, fine-grained phyllosilicate-aggregates. The close microstructural association of this transformation with secondary, syntectonic calcite indicates intense fluid migration during shearing. This process caused also a major change in the relative importance of deformation mechanisms, and—in turn—in bulk rheology: frictional processes were largely substituted by fluid-assisted viscous grain boundary sliding associated with solution creep resulting in a more ductile flow regime. An IWL_{vv}-structure (interconnected weak layer structure with apparently viscous rheologies both in the matrix and the boudins) was formed during this stage (cf. Fig. 3B), as both the macro- and microscale observations suggest negligible competence contrast between the newly formed aggregates and the fine-grained phyllosilicate-rich matrix in the consequence of the very similar phase-composition and grain-size.

In summary, the formation and evolution of the LSZ were basically controlled by (i) the precursor weak and anisotropic lithology (i.e. fine-grained, tuffaceous protolith being foliated during the early stage of the tectonometamorphic evolution), (ii) fluid influx into the shear zone leading to syntectonic reaction softening (feldspar → mica) which, in turn, caused (iii) a switch in bulk deformation as combined microfracturing and intergranular sliding (cataclasite-stage) were increasingly substituted by viscous sliding (VGBS) contributing to pronounced weakening (mylonite-stage).

4.3. Age and kinematic frame of the LSZ

Considering the K-Ar isotopic ages on white K-mica-rich, <2 μm grain-size fraction samples (Table 5), it is also obvious that there is no correlation between the intensity of deformation and the age values within as well as outside the LSZ. The average of all data (76.1 Ma; s = 1.8 Ma, $n = 10$) practically corresponds to the white K-mica K-Ar ages around 80 Ma (77–82 Ma) determined from the fine fractions of various metasedimentary and metaigneous rocks of the Eastern Bükk Mesozoic (Árkai et al., 1995a). A very similar K-Ar whole rock age (84 Ma) was obtained on a meta-andesite tuff at Lillafüred by Árva-Sós et al. (1987), too. Regarding also the same age and metamorphic grade of the control sample LF-X hosted in a low-strain domain of the studied metavolcanite series, it follows that the ages between 75–85 Ma record roughly the age of metamorphism, i.e. the early phase of cooling after the peak of anchi/epizonal, Late Cretaceous metamorphism (Fig. 8), as closing temperature of <2 μm white K-mica was determined about 260 ± 20 °C (Hunziker et al., 1986). Consequently, the obtained data about 76 Ma in the LSZ do not represent the age of late-phase, dextral shearing in the Eastern Bükk, in contrast to the conclusions of other studies (Dunkl et al., 1994; Árkai et al., 1995a; Csontos, 1999). This latter interpretation is also questioned by the results of Müller et al. (1999), emphasizing the methodical difficulties in dating of (very) low-grade fault rocks. The age of shearing can be, therefore, bracketed in the latest Late Cretaceous–Early Tertiary interval, as overlying, postorogenic sediments are dated to be Upper Eocene.

Another possibility is that shearing took place prior to, or roughly synchronously with the peak conditions of high-T anchizonal metamorphism. From a pure geochronological point of view one could expect namely ca. the same ages also in these cases, as a consequence of the coeval, post-tectonic recrystallization of white K-mica both in the heavily and weakly deformed rocks. However, the pervasive retrograde alteration of feldspar and phyllosilicate retrogression observed in the LSZ—both suggesting relatively "cold" conditions during shearing—do not support this scenario.

Structurally it is also obvious that the dextral activity of the LSZ must be younger than the penetrative F_2 folding, since shearing occurred along the pre-existing S_2 foliation (Fig. 2), formed as axial plane cleavage during F_2 folding. Furthermore, recent studies (Csontos, 1988, 1999; Mádai, 1995; Németh and Mádai, 2003, 2004) have shown that early F_2 folding was roughly contemporaneous with peak metamorphic conditions (occurred before 80 Ma in the Eastern Bükk), and later deformations occurred at considerably lower temperatures during cooling. This indirectly suggests that shearing along the LSZ proceeded as a late-stage, retrograde event during the Eoalpine tectonometamorphic cycle (Fig. 8).

Structural data (Fig. 3D) indicate pure to slightly oblique, dextral strike-slip kinematics in the LSZ, regarding also shear sense indicators with consistent top-to-the-E shearing. The deduced dextral shearing is compatible with the kinematics

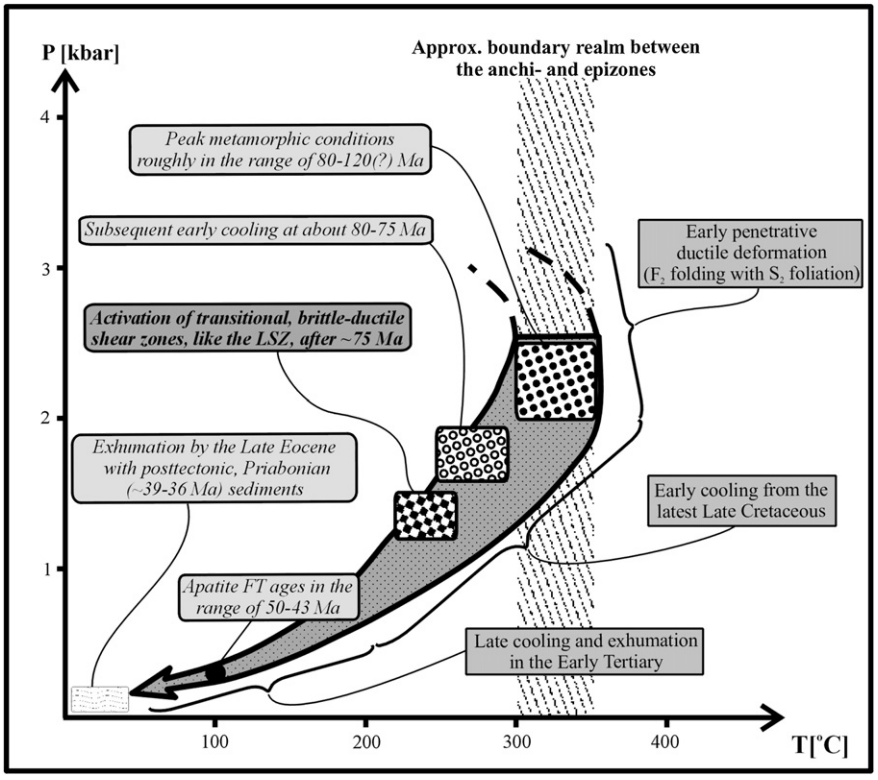

Fig. 8. Inferred tectonometamorphic evolutionary scheme of the Parautochthon unit involving also the LSZ in the Eastern Bükk. Sources of petrological-geochronological data: Árkai, 1973, 1983; Árkai et al., 1995a; this work.

postulated by Csontos (1988, 1999) on the similarly oriented Bükkszentkereszt Fault (BF; see Fig. 1A), located ca. 1.5–2 km south of the LSZ. This fault was assumed to be a Late Cretaceous, transitional semi-ductile, dextral strike-slip fault related to the post-folding arching of the major F_2 structures in the Eastern Bükk. Our results on the LSZ show that its dextral activity was related to the late stage of the tectonometamorphic evolution during cooling, too. Therefore, the LSZ might be genetically connected to the dextral shearing along the BF, considering also the occurrences of irregularly placed shear zones within the studied metavolcanite series which can be traced further to the south up to the BF (our unpublished data; Pelikán, pers. commun.). However, further detailed studies are needed in order to constrain the kinematics, spatial links and age of these shear zones in the whole Eastern Bükk Mts.

5. Conclusions

1. Although the studied fine-grained, tuffaceous metavolcanic rocks from the transitional brittle–ductile LSZ (Eastern Bükk Mts., NE Hungary) show a prominent mylonitic rock structure at hand-specimen scale, only a negligible amount of crystalplastic deformation was observed at the grain-scale, hence its contribution to the total bulk strain is negligible. Bulk deformation was predominantly accommodated by combined cataclasis (feldspar, opaque) and grain boundary sliding associated with solution mass transfer in the prevailing, fine-grained matrix phyllosilicates.
2. Intense fluid migration during shearing—evidenced by widespread synkinematic growth of fibrous calcite (±chlorite and quartz) along shear bands and between boudinaged mineral fragments—largely enhanced pervasive, syntectonic retrograde alteration of strong feldspars into weak, fine-grained phyllosilicate aggregates. This led to a pronounced strain weakening (with the formation of ultramylonites) in narrow zones as combined microfracturing and intergranular sliding were increasingly substituted by viscous grain boundary sliding associated with solution mass transfer. The evolution from a cataclasis-dominated deformation into a more ductile, mylonitic regime was basically controlled by fluid flow and increasing strain within the LSZ.
3. Largely inert petrological and geochronological parameters (illite and chlorite "crystallinity" indices, crystallite thickness and lattice strain data, chlorite-Al^{IV} thermometry, K-Ar ages on <2 μm white K-mica-rich fractions) indicate peak metamorphic conditions around the boundary of the anchi/epizone (300–350 °C) and subsequent early cooling at ca. 76 Ma both in the heavily sheared and the enclosing, weakly deformed, precursor rocks. None of the above parameters show any evidence for interaction with the intensity of shear deformation. The uniformity of these parameters—all reflecting crystal-lattice properties in some way—together with the products of phyllosilicate retrogression indicate that shearing in the LSZ must have been a relatively late and "cold" (≤250–270 °C), fluid-assisted process.
4. In contrast to previous interpretations, K-Ar ages in the range of 75–85 Ma from the Eastern Bükk are not regarded as the age of shearing along the LSZ (and other similar brittle–ductile shear zones), but they represent the approximate age of the transitional anchi/epizonal regional metamorphism (i.e. the early phase of cooling after peak conditions). Therefore, dextral activity of the LSZ must have occurred after ca. 76 Ma, in the latest Late Cretaceous–Early Tertiary interval.

Acknowledgements

The present work was financially supported by the Hungarian Research Fund (OTKA), Budapest by the grant T-049454/2005–2008 to P.Á. ("Characterization of prograde and retrograde metamorphic processes using the mineral structural and chemical changes of phyllosilicates and other rock-forming minerals"), No. F-047322/2004–2007 to P.H. ("Investigation of the relations between metamorphism and tectonic deformation") and No. T060695/2006–2009 and M041434/2002–2003 to K.B. The constructive reviews of L. Csontos and W. Frisch largely improved the quality of the original manuscript. W. Dunne is thanked for comments on a previous version of the manuscript. The valuable technical help of Zs. Koroknai and comments of P. Pelikán are gratefully acknowledged.

References

Abad, I., Guitierrez-Alonso, G., Nieto, F., Gertner, I., Becker, A., Cabro, A., 2003. The structure and the phyllosilicates (chemistry, crystallinity and texture) of Talas Ala-Tau (Tien Shan, Kyrgyz Republic): comparison with more recent subduction complexes. Tectonophysics 365, 103–127.

Árkai, P., 1973. Pumpellyite-prehnite-quartz facies Alpine metamorphism in the Middle Triassic volcanogenic-sedimentary sequence of the Bükk Mountains, Northeast Hungary. Acta Geologica Hungarica 17, 67–83.

Árkai, P., 1983. Very low- and low-grade Alpine metamorphism of the Paleozoic and Mesosoic Formations of the Bükkium, NE-Hungary. Acta Geologica Hungarica 26, 83–101.

Árkai, P., 1991. Chlorite crystallinity: an empirical approach and correlation with illite crystallinity, coal rank and mineral facies as exemplified by Palaeozoic and Mesozoic rocks of northeast Hungary. Journal of Metamorphic Geology 9, 723–734.

Árkai, P., Sadek Ghabrial, D., 1997. Chlorite crystallinity as an indicator of metamorphic grade of low-temperature meta-igneous rocks: a case study from the Bükk Mountains, northeast Hungary. Clay Minerals 32, 205–222.

Árkai, P., Balogh, K., Dunkl, I., 1995a. Timing of low-temperature metamorphism and cooling of the Paleozoic and Mesozoic formations of the Bükkium, innermost West Carpathians, Hungary. Geologische Rundschau 84, 334–344.

Árkai, P., Sassi, F.P., Sassi, R., 1995b. Simultaneous measurements of chlorite and illite crystallinity: a more reliable geothermometric tool for monitoring low- to very low-grade metamorphism in metapelites. A case study from Southern Alps (NE Italy). European Journal of Mineralogy 7, 1115–1128.

Árkai, P., Merriman, R.J., Roberts, B., Peacor, D.R., Tóth, M., 1996. Crystallinity, crystallite size and lattice strain of illite-muscovite and chlorite: comparison of XRD and TEM data for diagenetic to epizonal pelites. European Journal of Mineralogy 8, 1119–1137.

Árkai, P., Balogh, K., Frey, M., 1997. The effects of tectonic shear strain on crystallinity, apparent mean crystallite size and lattice strain of phyllosilicates in low-temperature metamorphic rocks. A case of study from the

Glarus overthrust, Switzerland. Schweizersche Mineralogische und Petrographische Mitteilungen 77, 27–40.

Árkai, P., Mata, M.P., Giorgetti, G., Peacor, D.R., Tóth, M., 2000. Comparison of diagenetic and low-grade metamorphic evolution of chlorite in associated metapelites and metabasites: an integrated TEM and XRD study. Journal of Metamorphic Geology 18, 531–550.

Árkai, P., Fereiro Mählmann, R., Suchý, V., Balogh, K., Sýkorová, I., Frey, M., 2002. Possible effects of tectonic shear strain on phyllosilicates: a case study from the Kandersteg area Helvetic domain Cetral Alps, Switzerland. Schweizerische Mineralogische und Petrographische Mitteilugen 82, 273–290.

Árva-Sós, E., Balogh, K., Ravasz-Baranyai, L., Ravasz, Cs, 1987. K/Ar dates of Mesozoic igneous rocks in some areas of Hungary. Annual Report of the Hungarian Geological Institute from the year 1985, 295–307 (in Hungarian).

Balen, D., Horváth, P., Tomljenović, B., Finger, F., Humer, B., Pamić, J., Árkai, P., 2006. A record of pre-Variscan Barrovian regional metamorphism in the eastern part of the Slavonian Mountains (NE Croatia). Mineralogy and Petrology 87, 143–162.

Balogh, K., 1964. Die geologischen Bildungen des Bükk-Gebirges. (Geological formations of the Bükk Mts.). Annals of the Hungarian Geological Institute 48, 2. Budapest. (in Hungarian).

Balogh, K., 1981. Correlation of the Hungarian Triassic. Acta Geologica Academiae Scientiarum Hungaricae 24, 3–48.

Bos, B., Spiers, C.J., 2001. Experimental investigation into the microstructural and mechanical evolution of phyllosilicate-bearing fault rock under conditions favouring pressure solution. Journal of Structural Geology 23, 1187–1202.

Bos, B., Peach, C.J., Spiers, C.J., 2001. Frictional-viscous flow of simulated fault gouge caused by the combined effects of phyllosilicates and pressure solution. Tectonophysics 327, 173–193.

Burkhard, M., 1993. Calcite-twins, their geometry, appearance and significance as stress-strain markers and indicators of tectonic regime: a review. Journal of Structural Geology 15, 351–368.

Burkhard, M., Badertscher, N., 2001. Finite strain has no influence on the illite crystallinity of tectonized Eocene limestone breccias of the Morcles nappe, Swiss Alps. Clay Minerals 36, 171–180.

Burkhard, M., Goy-Eggenberger, D., 2001. Near-vertical iso-illite-crystallinity surfaces cross-cut the recumbent fold structure of the Morcles nappe, Swiss Alps. Clay Minerals 36, 159–170.

Carosi, R., Leoni, L., Montomoli, C., Sartori, F., 2003. Very low-grade metamorphism in the Tuscan Nappe, Northern Apennines, Italy: relationship between deformation and metamorphic indicators in the La Spezia mega-fold. Schweizersche Mineralogische und Petrographische Mitteilungen 83, 15–32.

Cathelineau, M., Nieva, D., 1985. A chlorite solid solution geothermometer. The Los Azufres (Mexico) geothermal system. Contribution to Mineralogy and Petrology 91, 235–244.

Chester, F.M., Friedman, M., Logan, J.M., 1985. Foliated cataclasites. Tectonophysics 111, 139–146.

Csontos, L., 1988. Étude géologique d'une portion des Carpathes Internes: le massif du Bükk (Nord-est de la Hongrie). Ph.D. thesis, University of Lille, 327 pp.

Csontos, L., 1999. Structural outline of the Bükk Mts (N Hungary). Bulletin of the Hungarian Geological Society 129, 611–651 (in Hungarian with English abstract).

Csontos, L., 2000. Stratigraphic reevaluation of the Bükk Mts (N. Hungary). Bulletin of the Hungarian Geological Society 130, 95–131 (in Hungarian with English abstract).

Dunkl, I., Árkai, P., Balogh, K., Csontos, L., Nagy, G., 1994. Thermal modelling based on apatite fission track dating: the uplift history of the Bükk Mts. (Inner Western Carpathians, Hungary). Bulletin of the Hungarian Geological Society 124, 1–24 (in Hungarian with English abstract).

Filipović, I., Jovanović, D., Sudar, M., Pelikán, P., Kovács, S., Less, Gy, Hips, K., 2003. Comparison of the Variscan - Early Alpine evolution of the Jadar Block (NW Serbia) and ''Bükkium'' (NE Hungary) terranes; some paleographic implications. Slovak Geological Magazine 9, 23–40.

Fodor, L., 1989. Multiphase folding near Nagy-Ökrös hill in the Bükk Mountains, NE Hungary. Bulletin of the Hungarian Geological Society 118, 147–162.

Frey, M., 1987. Very low-grade metamorphism of clastic sedimentary rocks. In: Frey, M. (Ed.), Low-Temperature Metamorphism. Blackie, Glasgow, pp. 9–58.

Giorgetti, G., Memmi, I., Peacor, D.R., 2000. Retarded illite crystallinity caused by stress induced sub-grain boundaries in illite. Clay Minerals 35, 693–708.

Haas, J. (Ed.), 1995. Lithostratigraphic Units of Hungary. Triassic. Hungarian Geological Institute, Budapest (in Hungarian).

Handy, M.R., 1990. The solid-state flow of polymineralic rocks. Journal of Geophysical Research 96 (B6), 8647–8661.

Hunziker, J.C., Frey, M., Clauer, N., Dallmeyer, R.D., Friedrichsen, H., Flehmig, W., Hochstrasser, K., Roggwiler, P., Schwander, H., 1986. The evolution of illite to muscovite: mineralogical and isotopic data from the Glarus Alps, Switzerland. Contributions to Mineralogy and Petrology 92, 157–180.

Jowett, E.C., 1991. Fitting iron and magnesium into the hydrothermal chlorite geothermometer. GAC/MAC/SEG Joint Annual Meeting, Toronto. In: Program with Abstracts, 16. A62.

Kisch, H.J., 1989. Discordant relationship between degree of very-low-grade metamorphism and the development of slaty cleavage. In: Daly, J.S., Cliff, R.A., Yardley, B.W.D. (Eds.), Evolution of Metamorphic Belts. Geological Society Special Publications, 43, pp. 173–185.

Kovács, S., Szederkényi, T., Buda, Gy., Császár, G., Nagymarosi, A., 2000. Tectonostratigraphic terranes in the pre-Neogene basement of the Hungarian part of the Pannonian area. Acta Geologica Hungarica 43, 225–328.

Kranidiotis, P., MacLean, W.H., 1987. Systematics of chlorite alteration at the Phelps Dodge massive sulfide deposit. In: Economic Geology, 82. Matagami, Quebec. 1898–1911.

Kübler, B., 1968. Evaluation quantitative du métamorphisme par la cristallinité de l'illite. Bulletin du Centre de Recherches Pau - S.N.P.A. 2, 385–397.

Kübler, B., 1990. ''Cristallinité'' de l'illite et mixed-layers: breve révision. Schweizersche Mineralogische und Petrographische Mitteilungen 70, 89–93.

Langford, J.I., 1978. A rapid method for analysing the breadth of diffraction and spectral lines using the Voigt function. Journal of Applied Crystallography 11, 10–14.

Less, Gy., Gulácsi, Z., Kovács, S., Pelikán, P., Pentelényi, L., Rezessy, A., Sásdi, L. (Eds.), 2002. Geological Map of the Bükk Mountains. Map published by the Geological Institute of Hungary, scale, 1:50000.

Lin, A., 1997. Ductile deformation of biotite in foliated cataclasite, Iida-Matsukawa Fault, central Japan. Asian Journal of Earth Sciences 15, 407–411.

Lin, A., 1999. S-C catclasite in granitic rock. Tectonophysics 304, 257–273.

Mata, M.P., Giorgetti, G., Árkai, P., Peacor, D.R., 2001. Comparison of evolution of trioctahedral chlorite/berthierine/smectite in coeval metabasites and metapelites from diagenetic to epizonal grades. Clays and Clay Minerals 49, 318–332.

Mádai, F., 1995. Deformation patterns in the crystals of carbonate rocks from the eastern part of the Bükk Mountains (Northeast Hungary). Bulletin of the Hungarian Geological Society 125, 65–86 (in Hungarian with English abstract).

McCaig, A.M., Knipe, R.J., 1990. Mass-transport mechanism in deforming rocks: Recognition using microstructural and microchemical criteria. Geology 18, 824–827.

Merriman, R.J., Peacor, D.R., 1999. Patterns of very low-grade metamorphism in metapelitic rocks. In: Frey, M., Robinson, D. (Eds.), Low-Grade Metamorphism. Blackwell, pp. 61–107.

Merriman, R.J., Roberts, B., Peacor, D.R., 1990. A transmission electron microscope study of white mica crystallite size distribution in a mudstone to slate transitional sequence, North Wales, U.K. Contributions to Mineralogy and Petrology 106, 27–40.

Merriman, R.J., Roberts, B., Peacor, D.R., Hirons, S.R., 1995. Strain-related differences in the crystal growth of white mica and chlorite: a TEM and XRD study of the development of metapelitic microfabrics in the Southern Uplands thrust terrain, Scotland. Journal of Metamorphic Geology 13, 559–576.

Müller, W., Dallmeyer, R.D., Neubauer, F., Thöni, M., 1999. Deformation induced resetting of Rb/Sr and $^{40}Ar/^{39}Ar$ mineral systems in a low-grade,

polymetamorphic terrane (Eastern Alps, Austria). Journal of the Geological Society of London 156, 261–278.

Németh, N., Mádai, F., 2003. Early phase ductile deformation elements in limestones of the Eastern part of the Bükk Mountains I. Bulletin of the Hungarian Geological Society 133, 563–583 (in Hungarian with English abstract).

Németh, N., Mádai, F., 2004. Early phase ductile deformation elements in limestones of the Eastern part of the Bükk Mts. Part two: - Patterns of microstructure. Bulletin of the Hungarian Geological Society 134, 1–28 (in Hungarian with English abstract).

Nieto, F., Mata, M.P., Bauluz, B., Giorgetti, G., Árkai, P., Peacor, D.R., 2005. Retrograde diagenesis, a widespread process on a regional scale. Clay Minerals 40, 93–104.

Odin, G.S., Adams, C.J., Armstrong, L.R., Bagdasaryan, G.P., Baksi, K.A., Balogh, K., Barnes, I.L., Boelrijk, N.A.I.M., Bonadonna, F.P., Bonhomme, M.G., Cassignol, C., Chanin, L., Gillot, P.Y., Gledhill, A., Govindaraju, K., Harakal, R., Harre, W., Hebeda, E.H., Hunziker, J.C., Ingamells, C.O., Kawashita, K., Kiss, E., Kreutzer, H., Long, L.E., McDougall, I., McDowell, F., Mehnert, H., Montigny, R., Pasteels, P., Radicati, F., Rex, D.C., Rundle, C.C., Savelli, C., Sonet, J., Welin, E., Zimmermann, J.L., 1982. Interlaboratory standards for dating purposes. In: Odin, G.S. (Ed.), Numerical Dating in Stratigraphy. John and Wiley and Sons, Chichester New York Brisbane, pp. 123–149.

Pantó, G., 1951. Geology of the eruptive rocks between villages Diósgyőr and Bükkszentkereszt, Bükk Mts. Bulletin of the Hungarian Geological Society 81, 137–145 (in Hungarian).

Pantó, G., 1961. Mesozoic magmatism in Hungary. Annales of the Hungarian Geological Institute 49, 785–799 (in Hungarian).

Passchier, C.W., 1984. The generation of ductile and brittle shear bands in a low-angle mylonite zone. Journal of Structural Geology 6, 273–281.

Pelikán, P., Less, Gy., Kovács, S., Pentelényi, L., Sásdi, L. (Eds.), 2005. Geology of the Bükk Mountains. Explanatory Book to the Geological Map of the Bükk Mountains (1:50000). Geological Institute of Hungary, Budapest, p. 284.

Platt, J.P., 1984. Secondary cleavages in ductile shear zones. Journal of Structural Geology 6, 439–442.

Platt, J.P., Vissers, R.L.M., 1980. Extensional structures in anisotropic rocks. Journal of Structural Geology 2, 397–410.

Roberts, B., Merriman, R.J., 1985. The distinction between Caledonian burial and regional metamorphism in metapelites from North Wales: an analysis of isocryst patterns. Journal of the Geological Society of London 142, 615–624.

Roberts, B., Merriman, R.J., Pratt, W., 1991. The influence of strain, lithology and stratigraphical depth on white mica (illite) crystallinity in mudrocks from the vicinity of the Corris Slate Belt, Wales: implications for the timing of metamorphism in the Welsh Basin. Geological Magazine 128, 633–645.

Schmid, S.M., Handy, M.R., 1991. Towards a genetic classification of fault rocks: Geological usage and tectonophysical implications. In: Hsü, K.J., MacKenzie, J., Miller, D. (Eds.), Controversies in Modern Geology. Academic Press, London, pp. 339–362.

Schréter, Z., 1943. Geology of the Bükk Mountains. Annual Report of the Hungarian Royal Geological Institute from the year 1943 (Appendix), 378–411 (in Hungarian).

Sibson, R.H., 1977. Fault rocks and fault mechanisms. Journal of the Geological Society of London 133, 191–213.

Steiger, R.H., Jäger, E., 1977. Subcommission on geochronology: convention on the use of decay constants in geo- and cosmochronology. Earth Planetary Science Letters 12, 359–362.

Stipp, M., Stünitz, H., Heibronner, R., Schmid, S.M., 2002. The eastern Tonale fault zone: a 'natural labratory' for crystal plastic deformation of quartz over a temperature range from 250 to 700 °C. Journal of Structural Geology 24, 1861–1884.

Szentpétery, Zs., 1929. Eruptivserie im Savóstale bei Lillafüred. Acta Chemica. Mineralogica et Physica 1, 72–128.

Szentpétery, Zs., 1932. Quarzporphyr des Bagolyberges bei Lillafüred. Acta Chemica. Mineralogica et Physica 2, 81–150.

Szentpétery, Zs., 1935. Der eruptive Teil des Fehérkő bei Lillafüred. Matematischer und Naturwissenschaftlicher Anzeiger der Ungarischen Akademie der Wissenschaften 52, 253–286 (in Hungarian).

Szentpétery, Zs., 1936. Allgemeine Verhältnisse der Eruptivgesteine des Lillafüreder Szentistván-berges. Matematischer und Naturwissenschaftlicher Anzeiger der Ungarischen Akademie der Wissenschaften 54, 279–308 (in Hungarian).

Szoldán, Zs., 1990. Middle Triassic magmatic sequences from different tectonic settings in the Bükk Mts (NE Hungary). Acta Mineralogica-Petrographica 31, 25–42.

Teichmüller, M., Teichmüller, R., Weber, K., 1979. Inkohlung und Illit-Kristallinität-Vergleichende Untersuchungen im Mesoikum und Palaozoikum von Westfalen. Fortschritte in der Geologie von Rheinland und Westfalen 27, 201–276.

Velledits, F., 1999. Anisian terrestrial deposits in the sequences of the Northern Bükk Mts. (Anisian-Ladinian layers of the Alsó-Sebes-víz key-section and Miskolc 10. borehole=Zsófiatorony). Bulletin of the Hungarian Geological Society 129, 327–361 (in Hungarian).

Warr, L.N., Greiling, R.O., Zachrisson, E., 1996. Thrust-related very low grade metamorphism in the marginal part of an orogenic wedge, Scandinavian Caledonides. Tectonics 15, 1213–1229.

White, S.H., Burrows, S.E., Carreras, J., Shaw, N.D., Humphreys, F.J., 1980. On mylonites in ductile shear zones. Journal of Structural Geology 2, 175–187.

Wise, D.U., Dunn, D.E., Engelder, J.T., Geiser, P.A., Hatcher, R.D., Kish, S.A., Odom, A.L., Schamel, S., 1984. Fault-related rocks: Suggestions for terminology. Geology 12, 391–394.

Zang, W., Fyfe, W.S., 1995. Chloritisation of the hydrothermally altered bedrock at the Igarape Bahia gold deposit, Carajas, Brazil. Mineralia Deposita 30, 30–38.